7-16-2020

Experimental Investigation of Pressure-Swirl Atomizer Spray Stability with Addition of a Pre-Filming Surface

Ethan Hanson
ejh7624@rit.edu

Experimental Investigation of Pressure-Swirl Atomizer Spray Stability with Addition of a Pre-Filming Surface

Submitted By:
Ethan Hanson

A Thesis Submitted in Partial Fulfillment of the Requirements for the Degree of Master of Science in Mechanical Engineering

Rochester Institute of Technology
Rochester, NY
Department of Mechanical Engineering
Kate Gleason College of Engineering
7/16/2020

Approved By:

Dr. Steven Day _____
Department Head, Department of Biomedical Engineering (Thesis Advisor)

Dr. Michael Schertzer _____
Associate Professor, Department of Mechanical Engineering

Dr. Jennifer O'Neil _____
Assistant Professor, Department of Manufacturing and Mechanical Engineering Technology

Permission to Reproduce

I, Ethan Hanson, herby grant permission to the Wallace Memorial Library of Rochester Institute of Technology to reproduce my thesis in whole or in part. Any reproduction will not be for commercial use or profit.

7/16/2020

Acknowledgements

First, I would like to thank my advisor, Dr. Steven Day, for taking on my thesis project with an application outside of his research area and for allowing me to use space and equipment from his laboratory throughout this research. His guidance and support was instrumental in the completion of this project.

I would like to thank my family, friends and peers who contributed to the completion of this work. Specifically, I would like to thank Kailee Polimeni (AA Tech) for her assistance to manufacture the atomizers used for this research. I would also like to thank Kenneth Court (AA Tech), Curtis Harding (AA Tech), and Adel Mansour (Parker Hannifin) for providing me with guidance and technical mentorship.

Additionally, I would like to thank Advanced Atomization Technologies and RIT for providing resources for this project. Resources specific to the equipment used for the collection of data were provided by RIT. Other resources specific to the project were provided by Advanced Atomization Technologies. I am grateful for the financial support provided by both parties.

Finally, I would like to thank my parents Linda and John Hanson, for providing me with the support, motivation, and work ethic to complete this project.

Abstract

In a combustion environment, system instabilities and dynamic responses of components can have a major influence on performance, emissions, and product life. One of the key components in a combustion system are the fuel injectors which utilize instabilities to generate a well atomized fuel spray. In this work, a pressure-swirl atomizer was studied under steady state operation and oscillating pressure differential conditions to simulate a dynamic system input to the atomizer. Atomizer spray with and without the addition of a pre-filming surface was evaluated to determine the influence that a pre-filming surface has on the dynamic response of the liquid sheet near the atomizer exit. High-speed video was utilized to capture the response of the liquid sheet and quantify the instability. It was found that under steady state operating conditions, the pre-filming surface increased the atomizer flow number and discharge coefficient. When comparing spray edge variation, the atomizer without a pre-filming surface demonstrated an increasing spray edge variation with increasing pressure while the opposite trend was observed in the atomizer with a pre-filming surface. Under conditions with an oscillating pressure differential, additional spray edge variation was observed near field of the atomizer exit but was nonexistent further downstream indicating that the superposition of the fluid from pressure oscillation dissipated as it moved further from the atomizer exit and did not have an impact on wave growth in the liquid sheet.

Table of Contents

List of Figures

List of Tables

Nomenclature

$AA\ Tech$	(Advanced Atomization Technologies)
A_a	Air Core Area
A_p	Tangential entry passage cross-sectional area
A_o	Exit Orifice Area
C_d	Discharge coefficient
d_o	Exit orifice diameter
D_s	Swirl chamber diameter
FN	Flow number (dimensionally correct form)
FN_{US}	Flow number for water
FN^*_{US}	Flow number for calibration fluid
FPS	(Frames per Second)
h	½ Liquid film thickness
K	Atomizer Constant
l_t	Trumpet length
$\dot{m}_L$	Liquid mass flow rate
RIT	(Rochester Institute of Technology)
$PDPA$	(Phase Doppler Particle Anemometry)
PDA	(Phase Doppler Anemometry)
PIV	(Particle Image Velocimetry)
R_e	Reynolds Number
s	Specific Gravity
SMD	Sauter Mean Diameter
T	Liquid surface tension
t_f	Liquid film thickness
t^*_f	Liquid film thickness for calibration fluid
U	Liquid Velocity
u	Axial component of Liquid Velocity
X	Ratio of air core area to exit orifice area
ΔP_L	Atomizer pressure differential
v	Kinematic Viscosity
θ	Spray cone half-angle
θ_t	Trumpet angle half-angle
ρ_L	Liquid density

1.0 Introduction

The process of converting a liquid into a spray of smaller droplets through the process of atomization has been heavily studied with applications in various industries including agriculture, meteorology, medicine, and combustion [1]. Atomization uses the kinetic energy of the liquid to induce the disintegration of a liquid sheet or jet [1]. For applications involving the combustion of liquid fuels, atomization is a critical consideration that affects combustor performance. Ideal conditions for combustion involves atomization of the liquid into small droplet sizes to maximize surface area and achieve sufficient mixing of fuel and air [1], [2]. Insufficient atomization can result in poor ignition performance, an increase in pollutant emissions, higher operating costs, and reduced component life [1]–[3].

Atomization is influenced by the design of the atomizer. The atomizer is designed to inject the liquid at a high velocity relative to the surrounding air. Instabilities in the air-liquid interface promotes disintegration of the liquid into smaller ligaments and droplets. The focus of the research in this paper is a pressure atomizer design known as a Pressure-Swirl (Simplex) atomizer. A pressure-swirl atomizer imparts a swirling motion into the fluid. Upon exiting the atomizer orifice, the liquid forms a conical sheet. The spray distribution caused by a pressure-swirl atomizer can be described as a hollow-cone or solid-cone. A hollow-cone nozzle typically provides better atomization and so is preferred for many applications including combustion [1]. In the case of a hollow-cone spray, the centrifugal force on the fluid causes the liquid sheet to expand radially as it travels further from the atomizer exit. As the sheet expands, the sheet thins until surface tension forces and instabilities at the air-liquid interface cause the sheet to break up into ligaments and droplets [1], [2], [4], [5]. The typical spray produced by a pressure-swirl atomizer can be seen in Figure 1.

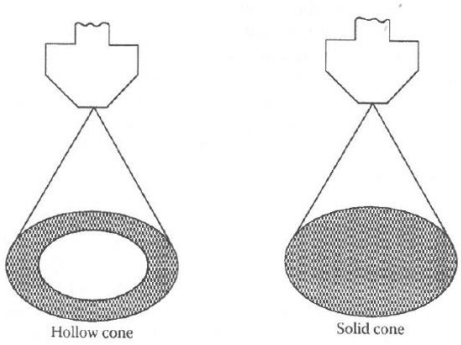

Figure 1: Spray Produced by Pressure-Swirl Atomizers from Lefebvre [1]

A pressure-swirl atomizer is designed with internal passages to generate the swirling liquid flow. Common pressure-swirl atomizer designs use tangential, axial, or conical slots to feed the liquid into a swirl chamber as shown in Figure 2. The liquid exits the swirl chamber through an orifice and the high angular velocity from the swirling motion causes the liquid to expand radially. The centrifugal force on the liquid while passing through the swirl chamber and orifice generates an air core in the center of the swirl chamber as shown in Figure 3 [1], [5]–[8].

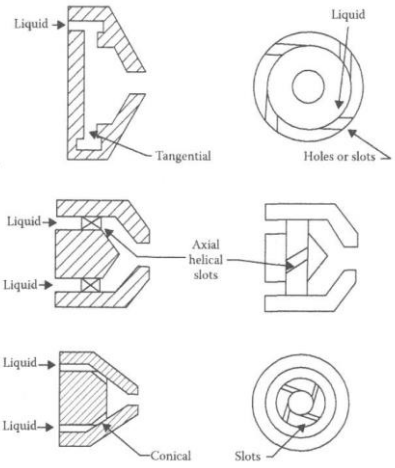

Figure 2: Various Designs of Pressure-Swirl Atomizers from Lefebvre [1]

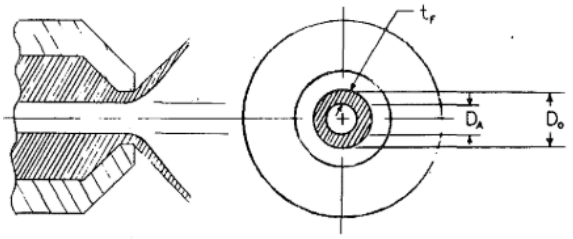

Figure 3: Schematic of a Hollow-Cone Pressure Swirl Atomizer from Simmons and Harding [9]

Due to the spray from a pressure-swirl atomizer being dependent on high angular velocity, various stages of spray development can be observed with increasing fluid pressure as shown in Figure 4.

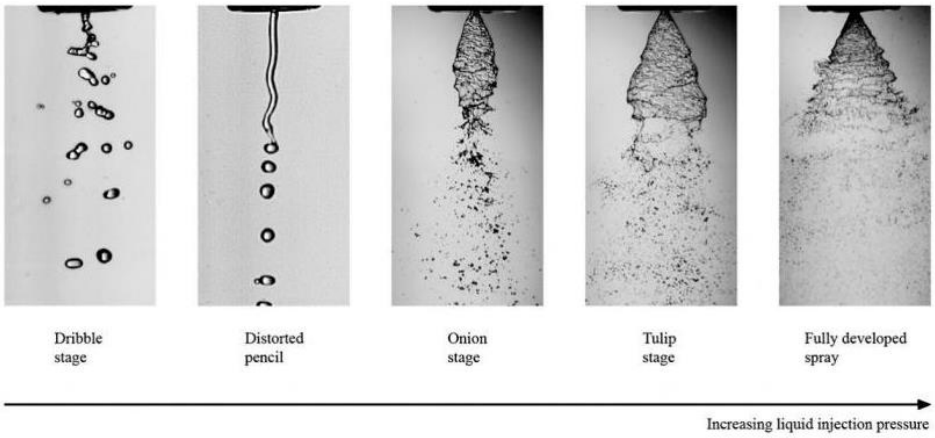

Figure 4: Stages in Spray Development with Increasing Liquid Injection Pressure [1]

There are several flow parameters that can be used to characterize an atomizer. The first is known as the Flow Number, FN_{US}. The flow number is used to relate the liquid mass flow rate of the atomizer to the overall pressure differential across the atomizer. The atomizer flow is measured experimentally and the Flow Number is calculated using Equation 1, where $\dot{m}_L$ is the liquid mass flow rate and ΔP_L is the atomizer pressure differential [1], [4]. It should be noted that while the typical standard in the aviation industry is to express atomizer flow number using Equation 1, it does not account for fluid type and is typically assumed to be calibration fluid. For the purposes of this paper, all flow numbers reported are for water as a working fluid. Flow number using calibration fluid will be represented by the symbol FN_{US}^{*}. The flow number can be modified to consider fluid effects by using Equation 2 where ρ_L is the liquid density [1].

$$FN_{US} = \frac{\dot{m}_L}{\sqrt{\Delta P_L}} \qquad \textit{Equation 1}$$

$$FN = \frac{\dot{m}_L}{\sqrt{\rho_L \cdot \Delta P_L}} \qquad \textit{Equation 2}$$

$$FN_{US} = 0.66 * 10^6 * \rho_L^{0.5} * FN \qquad \textit{Equation 3}$$

In Equation 2, the flow number is presented in m^2. Equation 3 can be used to calculate the flow number in $(lbm/hr)/\sqrt{lbf/in^2}$ as presented in Equation 1 [1][10]. The flow number is an important consideration when evaluating the required liquid mass flow rate and the pressure capacity of the fuel injection system. In the absence of experimental data, the flow number can be predicted based on atomizer dimensions. The equation derived by Rizk and Lefebvre is shown in Equation 4, where A_p is tangential entry passage cross-sectional area, D_s is the swirl chamber diameter, and d_o is the nozzle discharge diameter [1]. This relationship between flow number and the dimensions of the atomizer demonstrates that the flow number of the atomizer is expected to be constant for different operating conditions.

$$FN = 0.395\left(\frac{A_p^{0.5} d_o^{1.25}}{D_s^{0.25}}\right) \qquad \textit{Equation 4}$$

If the flow number is known, a discharge coefficient of the atomizer can be calculated. By expressing the mass flow rate in Equation 1 in terms of fluid velocity and utilizing Bernoulli's equation to solve for fluid velocity, the flow number can be re-written as shown in Equation 5 where A_o is the exit

orifice area, C_d is the atomizer discharge coefficient, s is the specific gravity of the working fluid, and FN_{US} is presented in units of $(lbm/hr)/\sqrt{lbf/in^2}$. The derivation of Equation 5 is documented in the appendix. Due to the air core limiting the flow area at the atomizer exit, the discharge coefficient for a pressure-swirl atomizer is typically low. Equation 5 demonstrates that for a given nozzle with a constant flow number, the discharge coefficient can also be expected to remain constant for various operating conditions.

$$FN_{US} = 19000 * A_o * C_d * \sqrt{s} \qquad \textit{Equation 5}$$

To predict spray cone angle, Giffen & Muraszew analyzed the flow in atomizers and generated an equation to predict the spray cone half angle in terms of the atomizer dimensions [1]. The equation to calculate the initial spray cone angle is shown in Equation 6 where θ is spray cone half-angle and K is the atomizer constant defined by Equation 7. The parameter X is defined by the ratio of the area of the air core to the orifice area and is shown in Equation 8 expressed in terms of the exit orifice diameter d_o and the liquid film thickness t.

$$\sin\theta = \frac{\frac{\pi}{2} C_d}{K\left(1 + \sqrt{X}\right)} \qquad \textit{Equation 6}$$

$$K = \frac{A_p}{d_o D_s} \qquad \textit{Equation 7}$$

$$X = \frac{\left(d_o - 2t_f\right)^2}{d_o^2} \qquad \textit{Equation 8}$$

The film thickness at the exit of the atomizer can be estimated using the equation derived by Simmons and Harding [9]. The equation to calculate the film thickness is shown in Equation 9, where FN^*_{US} is the atomizer flow number for calibration fluid and the film thickness is presented in microns. When used to calculate the film thickness of the liquid sheet at the exit of the orifice, the tangential component of the velocity can be neglected and so θ can be assumed to be zero. Simmons and Harding's derivation determined that the film thickness was independent of the differences between calibration fluid and water, therefore this equation can be reconfigured to solve for the film thickness of an atomizer by substituting the flow number for water and modifying the constant. Film thickness

calculated using the Equation 10 yields the same result for film thickness as Equation 9 except for rounding errors.

$$t_f^* = \frac{0.48\, FN_{US}^*}{d_o \cos\theta} \qquad \textit{Equation 9}$$

$$t_f = \frac{0.42\, FN_{US}}{d_o \cos\theta} \qquad \textit{Equation 10}$$

By using conservation of momentum, the axial component of the fluid velocity can be solved for. An expression for the axial velocity as a function of mass flow rate is shown in Equation 11 [1] where A_a is the area of the air core. By using Equation 1 and the assumption made by Simmons and Harding that $t_f \ll d_o$ [9], the axial component of the fluid velocity can be expressed in terms of the pressure differential as shown in Equation 12. Finally, knowing the axial component of the fluid velocity and the spray cone angle, the fluid velocity and Reynolds number at the exit orifice can be calculated using equations Equation 13 and Equation 14.

$$u = \frac{\dot{m}_L}{\rho_L (A_o - A_a)} \qquad \textit{Equation 11}$$

$$u = \frac{FN_{US}\sqrt{\Delta P_L}}{\rho_L \pi d_o t_f} \qquad \textit{Equation 12}$$

$$U = \frac{u}{\cos\theta} \qquad \textit{Equation 13}$$

$$R_e = \frac{t_f U}{v} \qquad \textit{Equation 14}$$

By demonstrating that the nozzle spray cone angle and flow number are dependent on atomizer geometry and constant for an atomizer, it can be inferred that for varying flow conditions, the nominal liquid film thickness exiting the atomizer will be constant. This is supported by the computational studies performed by Fu which concluded that the liquid film thickness at the nozzle exit was insensitive to changing ambient pressure [8]. For an atomizer with a constant FN under an operating

condition with an oscillating pressure differential, the mass flow rate and thereby fluid velocity must also vary to compensate. This periodic velocity change would result in fluid particles superimposing in a phenomenon referred to as the klystron effect [10]. The superposition of fluid creates thickening and thinning of the liquid sheet known as a varicose (symmetric) wave mode [11].

2.0 Research Question

How does the addition of a pre-filming surface impact the liquid film instability and spray of a pressure-swirl atomizer when exposed to oscillations in pressure differential across the atomizer?

3.0 Societal Context

Often, studies on atomizer sprays are done under ideal conditions. In a combustion application, there are numerous influencers that make the operation of an atomizer less than ideal. A product of the combustion process is the release of energy in the form of heat that can drive pressure fluctuations into the combustor environment [10]. These pressure dynamics can have negative impact on combustor components and drive fluctuations in the pressure drop across the atomizer. Changes in pressure drop across the atomizer can affect the performance of the atomizer by creating fluctuations in the mass flow rate. Changes in atomizer performance can impact the mass distribution, droplet sizes, fuel-air mixing, and combustion reaction thereby contributing to combustion instabilities in a feedback loop [10], [12]. In addition to combustion instabilities, sources of turbulence in fuel lines, pump fluttering, vibrations, and other influencers drive pressure perturbations into the atomizer from the upstream end [12]. To understand the coupling of a system of instabilities, the effect of instabilities on each component must be understood. Studies demonstrating the coupling of pressure differential oscillations and film instabilities of a pressure-swirl atomizer have been performed [6], [10].

In some applications, the maximum natural spray cone angle is not required or desired. In such applications, a pre-filming surface, or trumpet, can be added to achieve a desired spray cone angle [5]. In addition to controlling the spray cone angle, the addition of a pre-filming surface can assist in injecting the fuel in the right location for proper mixing [5] as well as creating a larger axial velocity component resulting in a greater jet penetration into the combustion environment. While the effect of a trumpet angle on atomizer characteristics has been studied by Xue et al. [5], the impact on spray stability has yet to be explored.

4.0 Literature Review

4.1 Atomization and Sprays

The text book written by Lefebvre and McDonell serves as an introduction to atomization and sprays [1]. Topics covered include atomization theories, atomizer designs, spray characteristics, and measurement techniques. The text provides a collection of equations from various sources to characterize both internal and external flow characteristics of pressure-swirl atomizers.

4.2 Experimental Evaluation of Low Pressure-Swirl Atomizer Applied Engineering Design Procedure

In the article submitted by Silvia Couto et al. to the *Journal of Propulsion and Power* [4], the spray from a Low Pressure-Swirl Atomizer was characterized using video and laser diffraction techniques. Spray characteristics evaluated include discharge coefficient, SMD, and spray angle. Characteristics were evaluated under various flow conditions created by a pressure differential across the atomizer. It was found that pressure conditions under 2 atm did not produce a practical spray to be used for evaluation. The spray produced under 2 atm produced a collapsed spray similar to that shown to be part of the collapsed regime or onion stage observed in other works including Reddy et al. [3]. For the full pressure range, experimental results were compared to predicted values calculated by the equations presented by Carlisle, Rizk and Lefebvre, and Jones. It can be observed from the results that lower pressure differential (1 to 3 atm) provides a closer match to Carlisle, while high pressure conditions (4 to 6 atm) matches better with the equations presented by Rizk and Lefebvre, and Jones.

To evaluate the SMD of the spray, a Malvern Mastersizer X laser scattering system was used. SMD measurements were taken for pressure conditions from 2 to 6 atm with good repeatability. When compared to the theoretical predictions presented in the paper, SMD predictions were within 10% of experimental data. This result was considered positive due to the simplicity of the model. It was noted that the SMD prediction for the 2 atm pressure condition represented an inverse (measured less than experimental) from other data points. This is attributed to the prediction's utilization of the assumption that the spray is fully developed. For pressure conditions from 3 to 6 atm, it was observed that experimental measurements were consistently lower than predicted. The likely origin of this discrepancy is the occurrence of secondary atomization (droplet breakup that occurs after initial ligament formation) which is not considered by the theoretical model.

Finally, measurements of spray angle were conducted using a Mavica-Sony MVC-FD97 camera. Experimental spray angle measurement results demonstrated a large difference from theoretical predictions at low pressure conditions, but converged with theoretical predictions at 6 atm. This discrepancy was attributed to the lack of a fully developed spray where the theoretical model assumed that the spray was fully developed. The paper references experimental results observed by Reddy and Mishra et. al [3] in which it was observed that spray angle in a non-fully developed spray increases with increasing pressure.

The results of this paper show that the equations established for discharge coefficient and SMD predictions can be used as a rough prediction for the behavior of an atomizer used for further research, but also demonstrated the challenges of using a simplified theoretical model to predict the spray angle in a developing spray. This is an important consideration when studying the instabilities of liquid film exiting a pressure-swirl atomizer as film instabilities are most dominant in an underdeveloped spray. This paper also considered the spray droplet size through SMD and a droplet volume distribution as resultant of the entire spray. However, the paper neglected to consider the effect of pressure differential on the spray patternation.

4.3 Experimental Investigation of a Pressure Swirl Atomizer Spray

In the article submitted by Marchione et al. to the *Journal of Propulsion and Power* [2], the behavior of the spray produced by a commercial pressure swirl atomizer was studied. Spray characteristics studied include droplet size, velocity component profiles, and cone angle variation. The experimental measurements were collected using a Phase-Doppler Anemometer (PDA) and a high-speed video camera.

The initial discussion of the experimental data addresses the measurements of droplet size and velocity measured by the PDA system. Plots of mean diameter and SMD, are shown. Both plots demonstrate an axially symmetric spray profile across the centerline of the spray which is expected of a hollow cone spray. Measurements were made at various distances from the exit of the atomizer. Both plots demonstrated similar trends with respect to the spatial distribution of droplets. The first trend observed was that the concentration of the largest droplet sizes increased radially with increasing axial distance from the atomizer exit. This is consistent with expectations of a cone shaped spray where droplets have a radial component of velocity when exiting the atomizer and, therefore, will move away from the centerline of the spray as axial distance increases. The second observation noted was that, with increasing axial distance, the mean diameter and SMD increased. This can be attributed to smaller droplets being pulled towards the center of the spray due to

aerodynamic effects generated by the spray resulting in a larger average droplet size towards the outer edge of the spray. Another possible contributor is evaporation of smaller droplets as the spray travels farther axially, thereby increasing the average droplet size.

The second part of the results discussion deals with the measurement of the spray cone angle. Spray cone measurements taken using the PDA measurement technique failed to indicate the fluctuating spray behavior of the atomizer due to measurements being taken over a time period of approximately 30 seconds. To study the fluctuating behavior of the liquid sheet, a high-speed camera was used. To evaluate the sampling frequency, results from spray measured using 3,000 frames per second and 10,000 frames per second were compared. While both plots showed the same average spray angle, it is notable that the higher frequency data plot showed a wider range for the maximum and minimum spray angle. By analyzing the power spectrum, it was determined that the principle component of the spray fluctuation was around 1790 Hz. Knowing the frequency of the spray fluctuations, it can be determined that 3,000 frames per second is below the Nyquist Frequency which results in aliasing of the data.

The key results of this paper demonstrate how to characterize the fluctuations of the liquid sheet exiting the atomizer and how to establish the required data recording frequency to sufficiently characterize the cone angle of the spray. The shortcomings of this paper are that it only evaluates the natural instability of the liquid sheet at a single pressure condition. This paper does not examine the source of the sheet instability or the instability of the liquid sheet at different stages in the spray development.

4.4 Studies on Spray Behavior of a Pressure Swirl Atomizer in Transition Regime

In the article submitted by Reddy et al. to the *Journal of Propulsion and Power* [3], the spray characteristics of a pressure-swirl atomizer are studied at multiple points during the transition regime of the developing spray. Measurements of discharge coefficient, cone angle, spray patternation, drop-size distribution, and SMD were taken. For the Reynolds number range measured, it was observed that there was no major change in discharge coefficient. To measure the spray cone angle, a laser sheet and charge-coupled camera were used. Time averaged images were analyzed using MATLAB's image processing toolbox. This method for measuring the spray cone angle does not capture instabilities in the spray angle. Results of the spray cone measurements are shown in Figure 5. By measuring the spray cone angle, the start of the developing spray region was identified. The developing regime of the spray was determined to begin when the applied pressure

(centrifugal force) was enough to overcome the surface tension forces that cause the spray angle to collapse. This is identified as the point when the cone angle begins to increase with increasing pressure. The collapse of the spray angle was further shown via the spray patternation results obtained using a mechanical patternator. Spray pattern results at 207 kPa showed the collapsed spray resulted in a concentrated mass distribution at the center of the spray, while results at 415 kPa demonstrated a hollow cone distribution. In addition to spray angle, the effect of increasing pressure on SMD was also measured and is shown in Figure 6. It can be observed that, in contrast to the spray cone angle, the SMD of the spray decreases with increasing pressure.

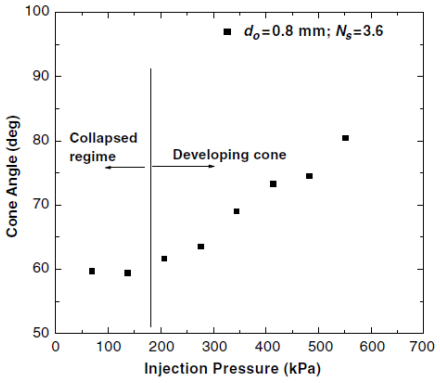

Figure 5: Effect of Injection Pressure on Spray Cone Angle [3]

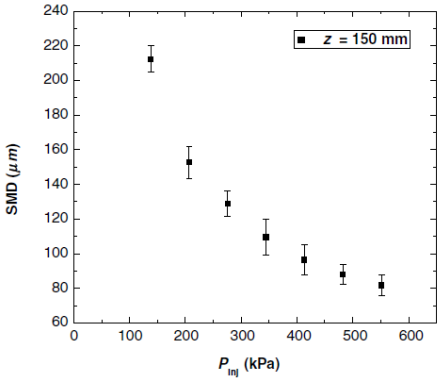

Figure 6: Effect of Injection Pressure on SMD [3]

The experimental results from this paper demonstrate the spray characteristics of a developing spray. The trends observed in cone angle and SMD measurements set an example for spray behavior of the atomizer in future work when operating in the collapsed and developing cone regime. The effects of this operation zone should be considered when evaluating spray characteristics near this regime.

4.5 Investigation of the Instability of a Moving Liquid Film

In the article submitted by Squire to the *British Journal of Applied Physics* [13], the instability of a 2-dimensional liquid film of constant thickness is analytically investigated and compared to the experimental observations of a pressure-swirl atomizer. For the purpose of this study, only the antisymmetric film oscillation mode was considered. The results of the investigation found that liquid film instability occurs for conditions with a Webber number, W_e, is less than 1. For the purposes of this work, the Weber number defined as shown in Equation 15 where T is the liquid

surface tension, ρ_L is the density of the liquid, U is the liquid velocity, and h is one half of the liquid film thickness.

$$W_e = \frac{T}{\rho_L U^2 h} \qquad \text{Equation 15}$$

This relationship indicates that as the fluid velocity or film thickness increases, the instabilities in the liquid sheet are driven by the antisymmetric mode, also described as wave motion. With respect to the proposed work, this is important to consider in that at low power or transition regime operation, the instability of the liquid sheet will likely be driven by the symmetric mode, or the thinning of the liquid sheet.

4.6 Dynamics of Radially Expanding Liquid Sheets

In the article submitted by Majumdar et al. to the *American Physical Society* [11], a liquid sheet was studied to demonstrate that the flapping of the liquid sheet is influenced by the thinning of the liquid sheet as it spreads from the nozzle exit. This statement contrasts previous work stating that the flapping was attributed to the interaction with the surrounding air and so neglected the effect of sheet thinning. To test, a laminar jet was impinged upon a vibrating impactor to generate a radially expanding liquid sheet. The frequency of the vibrating impactor was varied to generate multiple test conditions at 1 atm and 0.6 atm. As the liquid sheet expands radially from the impactor, the liquid sheet thickness decreases. If the claim that sinuous wave growth is dominated by the surrounding air, the wave growth would be expected to decrease with decreasing air pressure. Experimental results of the study, as shown in Figure 7, demonstrated that the decrease in air pressure had a negligible impact on the wave growth.

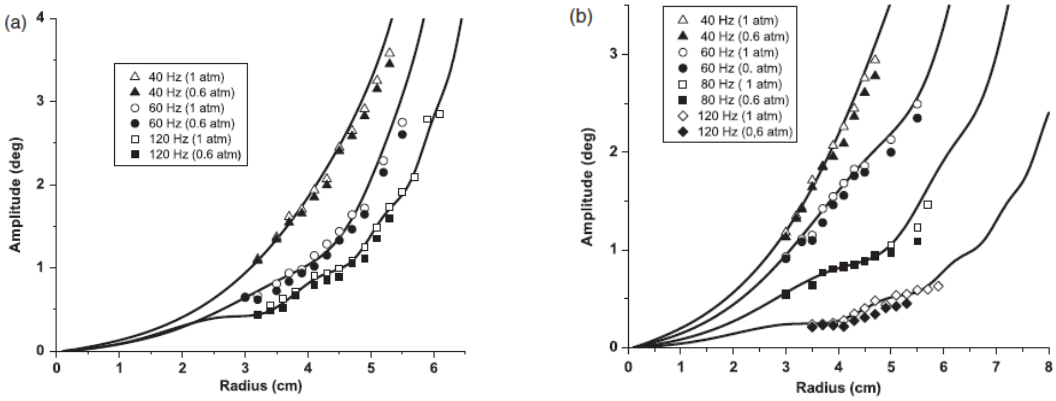

Figure 7: Measured Amplitude of Surface Inclination Angle at (a) Weber Number = 550 and (b) Weber Number = 700 [11]

These findings indicate that the sinuous wave growth is influenced by the thinning of the liquid sheet. An implication of this result is that the instability of the liquid sheet can be a function of the disturbances in the upstream system.

Although the work presented was performed on a flat liquid sheet, the findings could potentially be applied to the liquid sheet emanating from a pressure-swirl atomizer. The assertion that sinuous wave growth is a product of sheet thinning indicates that upstream pressure oscillations could promote sheet breakup of a pressure-swirl atomizer. In the context of combustion application, the work presented considers atmospheric and sub atmospheric pressures. In a combustion environment, air pressure and by association air density, would be higher than atmospheric and could increase the effect of the air on sinuous wave growth.

4.7 Periodic Atomization Characteristics of Simplex Swirl Injector Induced by Klystron Effect

In the article submitted by Yang et al. to the *Chinese Journal of Aeronautics* [10], the periodic response of a liquid film and atomization of a pressure-swirl atomizer was investigated experimentally. A hydrodynamic mechanical pulsator was utilized to apply pressure fluctuations upstream of the atomizer. For experimental measurements, a single operating condition was used with pressure fluctuations at 1±0.2 MPa. Fluctuation frequency was varied from 6.6 to 848.8 Hz. Experimental results demonstrated a response by the atomizer liquid film and spray between 0 to 300 Hz. It was also demonstrated that the pressure fluctuation correlated with the breakup length of the liquid sheet. This validates that atomizer pressure differences can impact the spray of the atomizer. However, the article does not investigate the effect on droplet size.

4.8 New Insights in the Primary Breakup Process of Prefilming Airblast Atomizers by SPH Predictions

In the article submitted by Holz et al. to the *International Conference on Liquid Atomization and Spray Systems* [14], the primary breakup of a prefilming airblast atomizer is investigated through simulation. The geometry considered consists of a prefilming surface with a liquid film on one side. Airflow above and below the prefilming surface travels in the same direction as the liquid film. Momentum from the faster flowing air drives the formation of waves in the film. At the trailing edge of the prefilming surface, the liquid film separates from the surface and forms ligaments that becomes atomized. The results of the simulations revealed three potential wetting modes at the trailing edge of the prefilming surface. The three wetting modes, shown in Figure 8, are described

as non-wetting, unstable accumulation, and stable accumulation. In the condition of non-wetting, the bulk of the fluid wave separates from the trailing edge with a small amount of fluid remaining on the trailing edge. In the unstable condition, the first wave is elongated while still attached to the trailing edge until the momentum from a second wave forces the breakup from the trailing edge. In the stable accumulation condition, the first wave fully wets on the trailing edge until a second wave reaches the trailing edge and induces breakup.

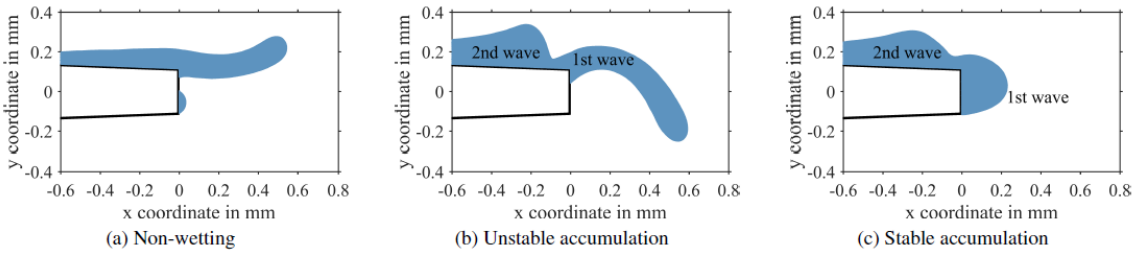

Figure 8: Wetting Modes of Trailing Edge from Holz et al. [14]

The work presented considers film waves initiated by co-flowing airflow in an airblast atomizer application. In the test conditions put forth in this proposal, waves in the liquid film would likely be initiated by upstream pressure instabilities. While not directly described by this work, a non-wetting condition would likely result in the smallest droplet sizes. It was also noted by this work that a non-wetting condition represents the strongest relationship between waves and the initial breakup, whereas the unstable accumulation and stable accumulation results in decoupling of the relationship between film waves and the initial breakup. For potential test hardware a sharp trailing edge would promote liquid separation and a non-wetting condition. This condition would likely yield the best experimental results.

4.9 Some Effects of Using Water as a Test Fluid in Fuel Nozzle Spray Analysis

In the article submitted by Simmons and Harding to the *Journal of Engineering and Power* [9], the effect of working fluid on atomizer performance was studied. The experimental results of the paper demonstrated that at comparable atomizer pressure differentials, the SMD of water is consistently higher than that of a kerosene type calibration fluid (MIL-PRF 7024). However, by normalizing the SMD and Weber number to the critical Weber number, it was possible to predict the performance of an atomizer with Kerosene type fuel using results obtained using water as the working fluid.

The paper also demonstrates a derivation of the predicted liquid film thickness in the atomizer exit orifice. It was shown analytically that the liquid film thickness is independent of the fluid property differences between water and kerosene. The film thickness is shown in Equation 9. This equation can be modified to apply for applications using water as the working fluid.

4.10 Effect of Geometric Parameters on Simplex Atomizer Performance

In the article submitted by Xue et al. to the *American Institute of Aeronautics and Astronautics Journal* [5], the effect of atomizer geometry on atomizer performance is computationally studied. Among the geometries considered, atomizer trumpet angle and length are studied. While studying the effect of trumpet angle, the trumpet length was kept constant. As trumpet angle was increased, it was noted that the film thickness at the atomizer exit decreased as expected. At the largest trumpet angle tested ($\theta_t = 40°$) the spray cone angle matched the trumpet angle. However, as the trumpet angle was decreased, the spray cone angle no longer matched the trumpet angle. While testing the effect of trumpet length, trumpet angle was held constant. As expected, with increasing trumpet length the film thickness decreases. It was also noted that as the trumpet length increased, the spray cone angle decreased. This is a result of a loss of angular momentum as the trumpet diameter increases with trumpet length. It was observed that the atomizer discharge coefficient was constant for all trumpet angles and lengths, indicating that the addition of a trumpet does not have any impact on the atomizer flow number.

The results demonstrated by this paper serves to establish expectations for the effect that the addition of a trumpet will have on the steady state atomizer performance. However, the scope of this investigation does not consider the effect of pressure instabilities on the atomizer performance.

4.11 Effects of Injection Pressure on Spray Atomization Characteristics with Measurement Technique Cross-Validation

In the article submitted by Lee et al. to the *International Conference on Liquid Atomization and Spray Systems* [15], the breakup characteristics of a pressure-swirl atomizer was studied experimentally. Two atomizers with different flow numbers were studied using shadowgraph, PIV, and PDPA methods. Spray characteristics matched trends observed in other papers discussed. The three measurement methods were compared using droplet diameter and velocity measurements at a common operating condition. Measurements were taken along the vertical axis of the spray and

were evaluated for the three zones of the spray: primary breakup, secondary breakup, and droplet coalescence.

For PIV measurements, a large spray density in the primary and early secondary breakup zones prevented measurements from being taken. Close to the end of the secondary breakup and the droplet coalescence zone, PIV velocity measurements are more consistent with other measurement methods. PDPA measurements were possible in the early stages of the spray, however due to ligament formation and irregular droplet sizes, measurement confidence was not high. PDPA measurements yielded a larger droplet size compared to shadowgraph techniques in early stages of the spray. PDPA measurement confidence was highest in the secondary spray zone before droplet coalescence occurred. Shadowgraph droplet size measurements were only limited by image resolution and so a high zoom lens was used limiting the field of measurement. It was found in the early stage of the spray, shadowgraph under predicted the droplet size compared to PDPA, but over predicted the droplet size in the droplet coalescence zone. In the droplet coalescences zone, over prediction of the droplet size was attributed to a lack of samples compared to PDPA measurements.

Overall, this paper demonstrated that droplet size measurements can be accomplished with different measurement techniques, however it is important to note the spray behavior at the point of measurement to determine the accuracy of the measurement. For the proposed research, droplet size measurement will likely be taken in the secondary atomization zone, indicating that based on the results of this paper PDPA is the measurement technique that will yield the most accurate results.

4.12 Experimental Study Swirl Injector Dynamic Response Using a Hydromechanical Pulsator

In the article submitted by Ahn et al. to the *Journal of Propulsion and Power* [6], dynamic response of a supersized swirl injector was designed. The injector geometry was designed to create a lengthened swirl chamber and air core length. To achieve a pulsating flow, an inlet cap with 16 tangential inlet holes was rotated by an electric motor. As the cap rotates, the inlet holes are aligned with the chamber holes periodically allowing flow into the swirl chamber. Measurements of spray angle response demonstrated peak responses at two resonant frequencies but did not change the average cone angle. Observations were also made to demonstrate a dynamic response to the air core diameter and the presence of a traveling wave. It should be noted that the method used to generate a dynamic response effectively created a variable flow number nozzle. According to the film thickness derived by Simmons and Harding [9], this would drive a changing film thickness.

The paper states that the air core diameter changed up to 4.5%. In addition, it is noteworthy that the researchers chose to orient their test setup to spray in a horizontal direction and ignore the effects of gravity. This is contrary to other spray measurements in which the atomizer is oriented to spray vertically downwards.

4.13 Measuring Air Core Characteristics of a Pressure-Swirl Atomizer via a Transparent Acrylic Nozzle at Various Reynolds Numbers.

In the article submitted by Lee et al. to the *Experimental Thermal and Fluid Science Journal* [7], the air core characteristics of an atomizer was studied as a function of Reynolds number. It is noted by the author that the atomizer studied utilized a single tangential inlet port resulting in a weaker swirling strength. The experimental results indicated an unstable regime at low Reynolds numbers where the air core had not developed and a transition regime in which the air core begins to develop but does not extend the full length of the swirl chamber. The underdeveloped air core resulted in a change in spray cone angle between unstable and stable air core regimes. This can be correlated with a decrease in atomizer discharge coefficient as the air core begins to develop.

The results of this paper indicated that it will be important to avoid operating conditions with low flow rates prior to the development of the air core. Measurements of spray angle in this regime will be inconsistent with higher flow conditions.

4.14 Numerical Simulation of the Internal Flow of Swirl Atomizer under Ambient Pressure

In the article submitted by Fu to the *Journal of Mechanical Engineering Science*, the internal flow of an open-ended swirl injector was studied using CFD. Simulation results revealed that the liquid axial and swirl velocity components were at a maximum at the interface with the air core. It was also observed that both velocity components decreased with axial distance due to the loss of momentum due to friction with the injector wall. When exposed to increasing ambient pressure the air core diameter increased. However, it was noted that the increase in air core diameter was too small to impact experimental measurements and therefore film thickness would be insensitive to air pressure. The change in air core diameter can likely be attributed to a changing nozzle flow number similar to the research conducted by Ahn et al. [6]. The inlet boundary condition for simulations was set at a constant flow rate. This creates a reducing flow number as ambient pressure increases and results in a reduction in film thickness. Predictions of spray cone angle were generated based on axial and swirling velocity components with respect to radius. Due to minor

changes in velocity components, it was determined that with increasing ambient pressure the spray cone angle would effectively remain constant.

When exposed to an oscillating ambient pressure, the author proposes that the pressure changes would drive surface waves in the liquid-air interface. However, these would present difficulties to monitor through simulation and so the effect on mass flow rate was observed instead. It can be observed from the data plots that the mass flow rate oscillations are phase delayed from the ambient pressure oscillations.

The results presented in this article demonstrates the expected velocity profile of the liquid film and air core inside a swirling flow injector and can be applied to a pressure-swirl atomizer. Changes to the air core diameter are likely to be negligible experimentally, however they could have a minor impact on the sheet stability. The scope of the article did not cover the impact of an oscillating ambient pressure on the axial and swirl velocity components.

4.15 Waves in Thin Liquid Films

In the paper by Santner [16], the decay of a capillary wave in a thin film is derived based on the Navier-Stokes equations. The resulting equation demonstrates that surface tension forces cause the wave amplitude to decay over time. It is also noted that waves with a lower wave length (or higher frequency) decay at a faster rate.

With application to the spray of a pressure-swirl atomizer, the decay of film waves can be applied to the film thickness on the prefilming surface. It can be expected that as the film thickness waves travel along the prefilming surface, the waves will decay resulting in a less severe thickness modulation at the atomizer exit. The expected implication is that this will result in a more stable spray than for applications without a prefilming surface.

5.0 Experimental Setup & Procedures

5.1 Experimental Setup

The experimental setup for this investigation was designed to spray vertically downward into a collection bin. A pressure vessel was used as a fluid reservoir in an air over water configuration and pressurized to approximately 90 psi using shop air. Due to safety concerns and ease of access, water was used for the working fluid instead of calibration fluid which is typically used for aerospace applications. The fluid was routed through ball and needle valves for flow control and were manufactured by Parker Hannifin. The fuel line was then routed through a vibration apparatus which was used to apply pressure oscillations by compressing the fuel line at a desired frequency. The vibration was controlled by a Type 4809 Vibration Exciter manufactured by Brüel & Kjær. The vibration exciter was powered by a power amplifier and controlled via a function generator. A v-block fixture was designed and attached to the top of the vibration cylinder to hold the fuel line in place as the fuel line was compressed against a cross-over bar. Due to challenges applying the required pressure oscillation, a section of larger diameter soft tubing was added to the fuel line that was easier for the vibration apparatus to compress. Finally, the fuel line was routed to the atomizer fixture where the pressure was measured by a pressure transducer.

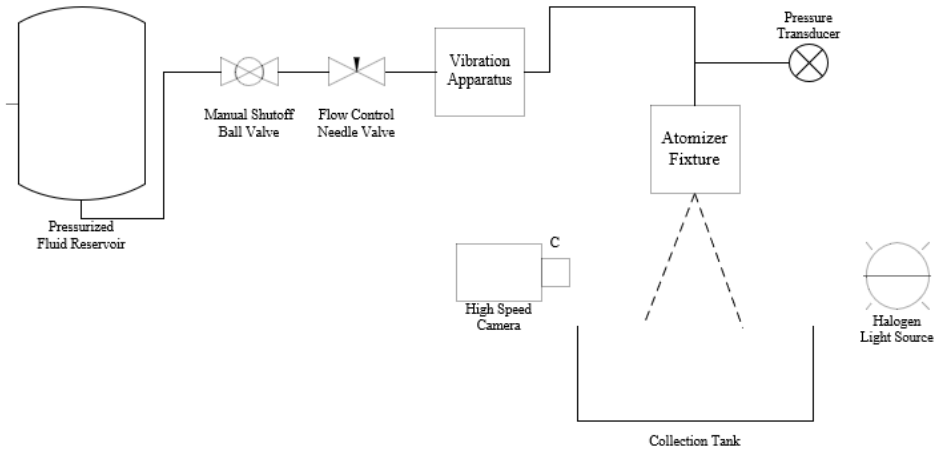

Figure 9: Experimental Setup Schematic

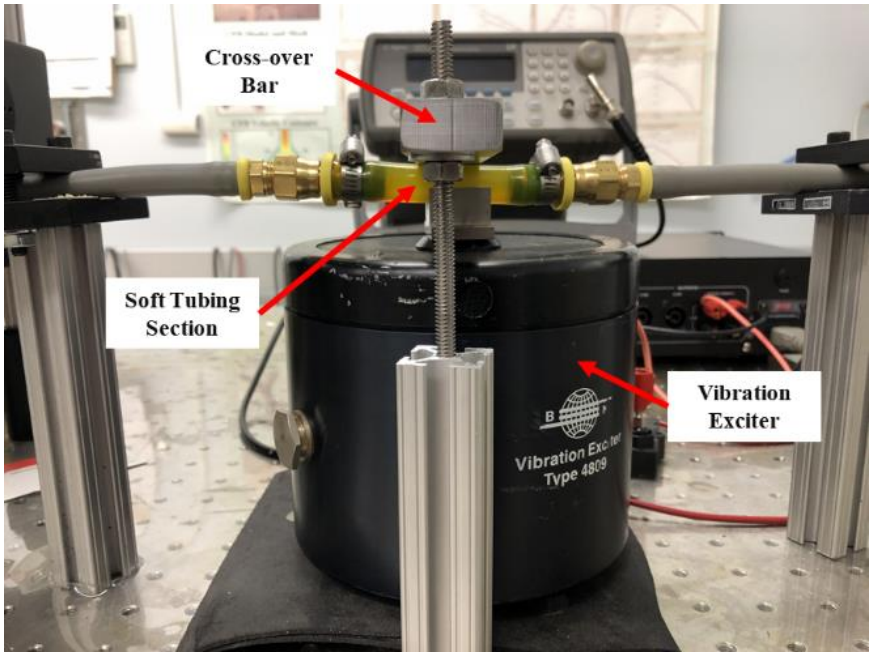

Figure 10: Vibration Apparatus

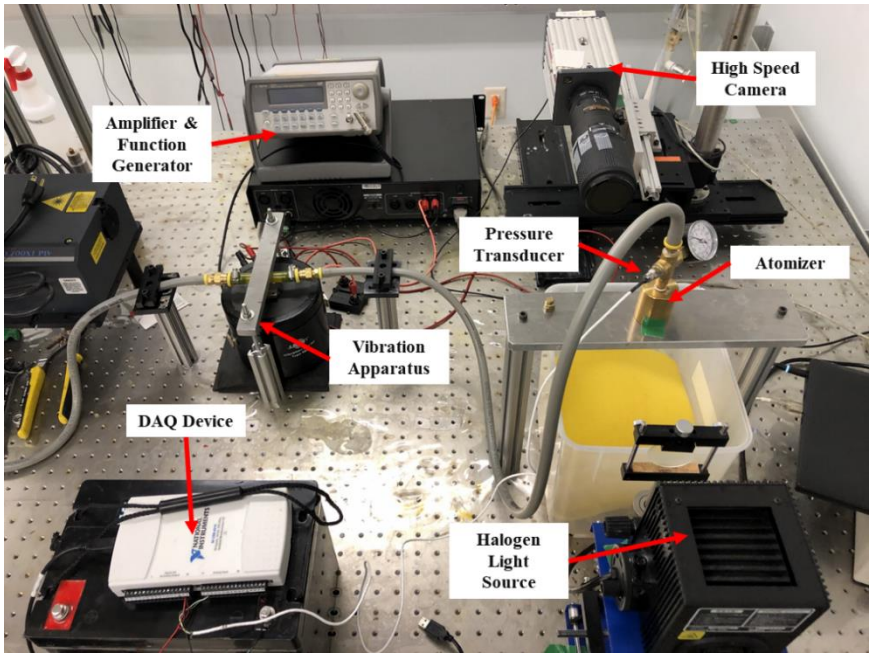

Figure 11: Photo of Test Setup (Fluid Reservoir and Flow Control Not Pictured)

Fluid pressure was measured just upstream of the atomizer using a pressure transducer Model Number XTL-190S-500SG manufactured by Kulite Semiconductor Products Inc. To calibrate the pressure transducer response, an analog dial pressure gauge was used to set a known pressure. Pressure transducer response measured in mV was recorded. During the calibration, it was found that the analog dial pressure gauge contained an offset from the true pressure, however the offset was determined to be consistent throughout the working range of the gauge. Therefore, a known pressure condition of 0 psi (1.23 mV transducer response) was used to anchor the pressure curve.

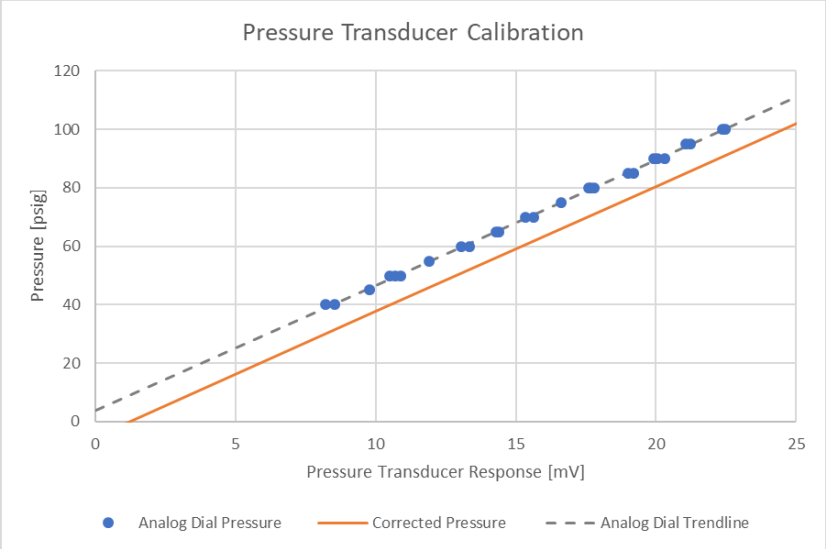

Figure 12: Pressure Transducer Measurement Calibration

Pressure data was recorded using a LabVIEW NI DAQ device and sampled at a rate of 10kHz. Pressure signal was filtered using a LabVIEW filter express VI. The filtering type chosen was smoothing with an exponential average time constant of 0.001. A LabVIEW Amplitude and Level Measurements express VI was used to display the nominal pressure and peak-to-peak pressure variation as a percentage of nominal pressure that was used to set flow conditions prior to collecting spray images. Nominal pressure was always set to within ±1 psid of the target pressure condition.

The high-speed camera used to capture the spray images was a Motion Pro X3 camera with a Nikon AF FX Micro-NIKKOR 200 mm camera lens. IDT Vision Motion Studio software was used to perform the image capture. Images were captured at a rate of 1000 frames per second (FPS) and a 2 µs exposure time. The spray was backlit by a 100 W halogen light source. The camera region of interest was limited to a 1024x720 pixel area. Each data set taken consisted of 2000 images.

Prior to the start of spray testing, a calibration image of a standard ruler (Figure 13) was used to determine the size of each image pixel. The straight-line distance between two points of a known distance (represented by dotted line shown in the figure) was measured using Image J software. A total of 20 repeat measurements were taken to establish a degree of confidence. The pixel size was determined to be 444.5 ± 2 µin [11.29 ± 0.051 µm].

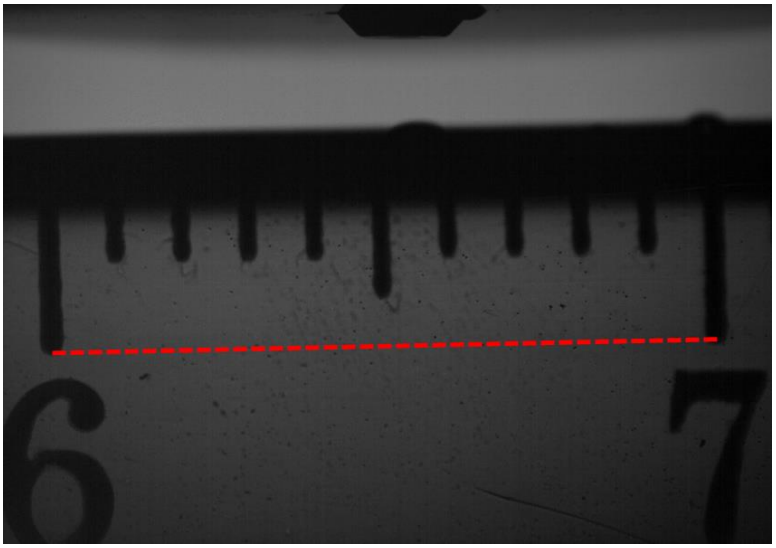

Figure 13: Calibration Image

The atomizer design used for this investigation was a simplex pressure swirl atomizer with three conical swirl slots. Two atomizer designs were manufactured by Advanced Atomization Technologies (AA Tech). The first, referred to as "Atomizer A", consisted of an orifice without any additional pre-filming surface that results in a natural spray angle. The second atomizer, referred to as "Atomizer B", utilizes a pre-filming surface to control the spray angle. The pre-filming surface for Atomizer B was designed to be near to the natural spray angle of Atomizer A, however the cone angle of the pre-filming surface was required to be slightly narrower than the natural spray angle to ensure that the liquid sheet adhered to the surface. Both atomizers use the same swirl plug to reduce potential inconsistencies between the atomizer flows. A side by side comparison of the two atomizers is shown in Figure 14. A close-up overlay of the atomizer exit orifices along with the coordinate system origin is shown in Figure 15.

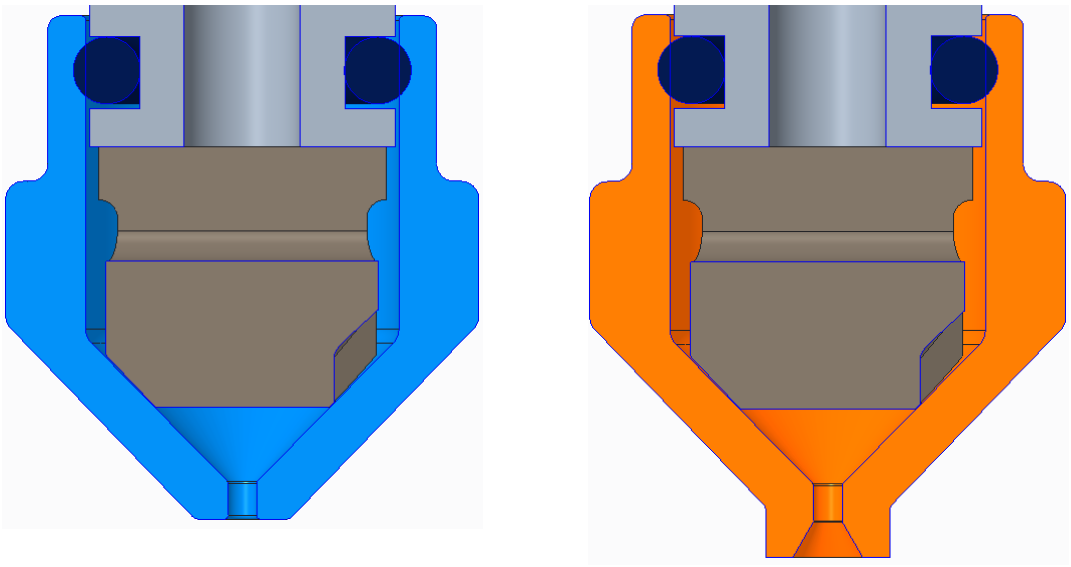

Figure 14: Side by Side Atomizer Geometry Comparison of Atomizer A (left) and Atomizer B (right)

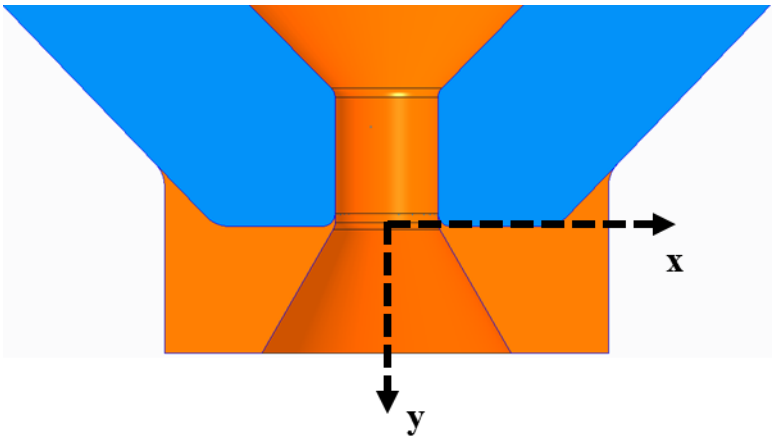

Figure 15: Atomizer Exit Orifice Overlay and Coordinate System Origin

5.2 Image Processing Procedure

All image processing was done using MATLAB. Prior to collecting images of the atomizer spray, a background image was taken to use as a baseline. If spray image captures extended across multiple days or the atomizer was removed from the test setup for any reason, a new background image was taken for the upcoming spray image sets. An example of a background image for each atomizer is shown in Figure 16.

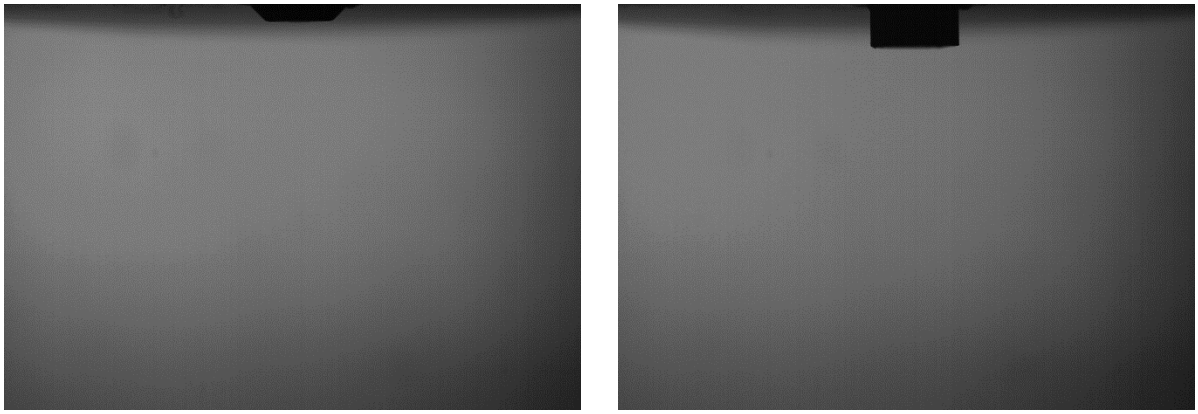

(a) (b)

Figure 16: Example Background ("baseline") Images for Atomizer A (a) and Atomizer B (b)

For a given image set, each image is loaded into MATLAB. An example of the raw spray image uploaded to MATLAB is shown in Figure 17. Next, the corresponding background image was used to normalize the spray image and a 2-D Gaussian filter is applied over the entire image. An example of the normalized and filtered image is shown in Figure 18. Finally, each pixel of the filtered image is evaluated against a threshold value and binarized. An example of the final binarized spray image is shown in Figure 19.

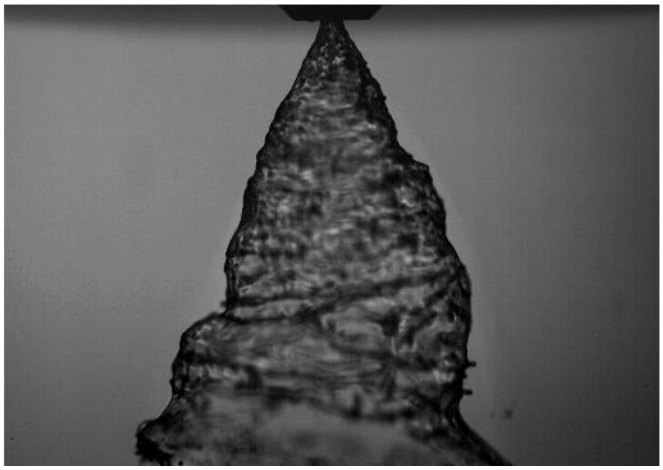

Figure 17: Raw Spray Image Uploaded to MATLAB

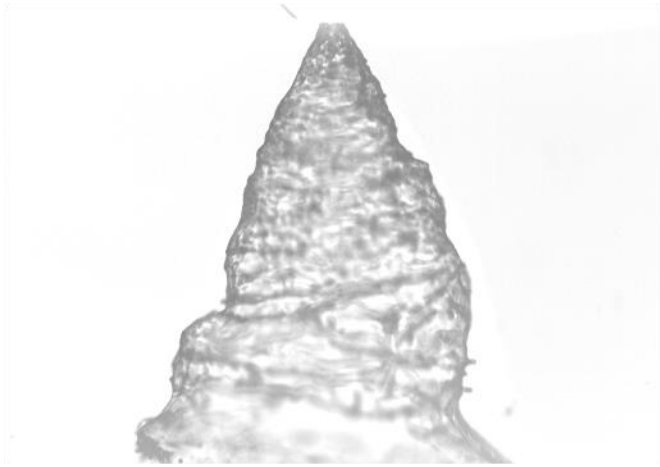

Figure 18: Filtered Spray Image

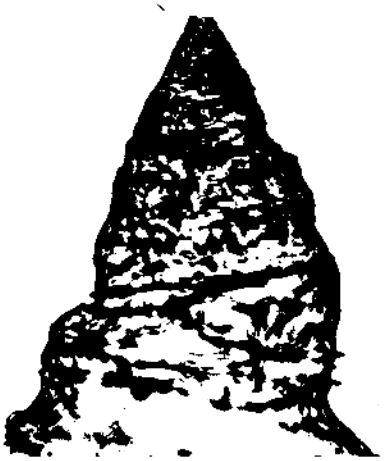

Figure 19: Binarized Spray Image

The spray edge was evaluated at four axial distances set from exit of Atomizer A. For consistency, the same axial locations were also used to evaluate Atomizer B spray. An overlay showing the y-origin and each spray edge measurement location is shown over the raw spray image for each atomizer in Figure 20 and Figure 21. It should be noted that due to the additional length of the pre-filming surface, the axial locations for Atomizer B are closer to the point that the fluid separates from the atomizer features than with Atomizer A.

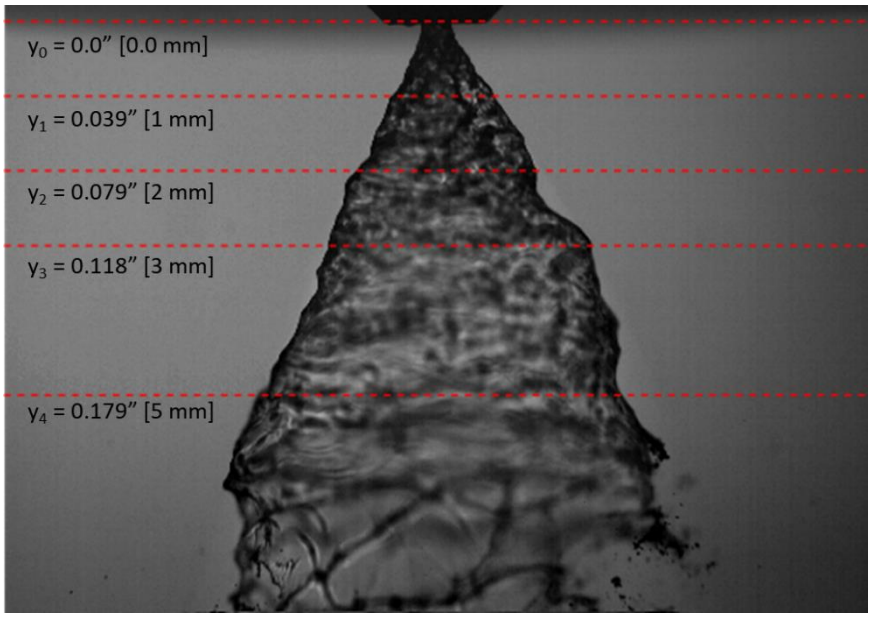

Figure 20: Spray Edge Measurement Locations of Atomizer A

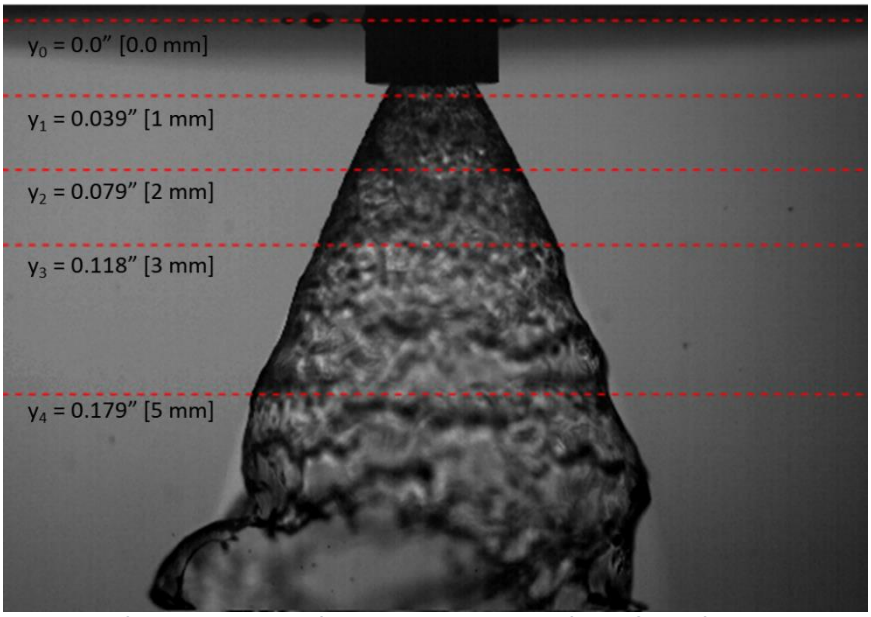

Figure 21: Spray Edge Measurement Locations of Atomizer B

Due to the nature of the turbulent air around the liquid spray, there can be a significant number of recirculating droplets that could potentially interfere with the edge detection algorithm. To mitigate the risk of a false edge detection, the MATLAB “remove outliers” function using the mean method (removes points outside of 3 standard deviations from mean value) was applied to identify and remove erroneous data points. Figure 22 shows the rejection rate for each set of images used in this investigation. Empty set numbers represent image sets that were not utilized. Except for two image sets at one spray location, rejection rate of spray edge was approximately 2% or less. Both image sets that contained a location with a rejection rate significantly larger than the rest of the population occurred at the right edge spray location closest to the atomizer exit. Both cases were investigated manually, and it was found that the spray edge was consistent to the point that the edge detection with outlier removal did not detect any change in the spray edge (standard deviation of zero). This indicates that in these two situations, the resolution of the field of view was not sufficient to detect the variation in the spray edge. After manually checking the data for these two image sets at that position, it was determined that all data points were within a reasonable range and so the “remove outliers” function was not applied to those data sets at that location.

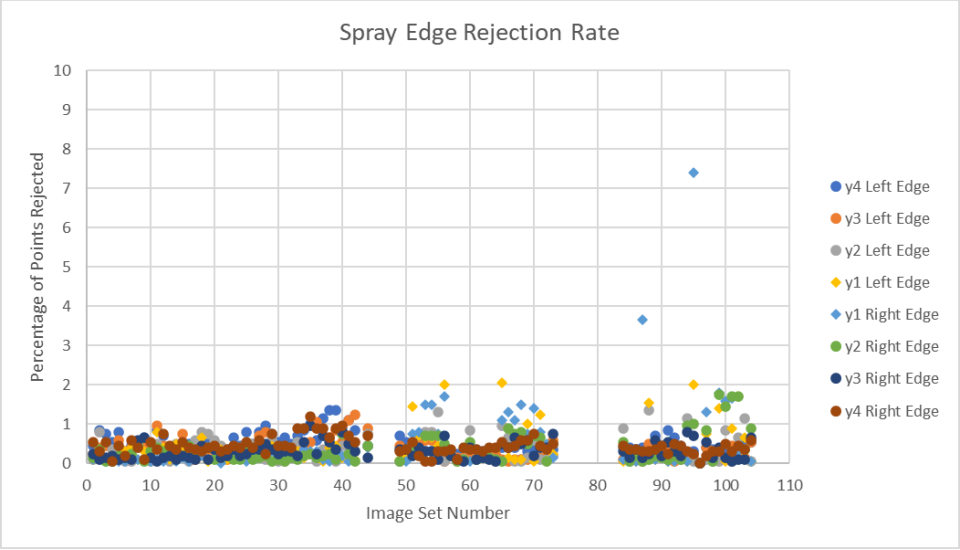

Figure 22: Spray Edge Rejection Rate

6.0 Results and Discussion

6.1 Atomizer Characterization at Steady State Operating Conditions

Atomizer sprays were characterized at various pressures between 10 and 70 psi. A side by side comparison of the raw spray images for both atomizers is shown in Figure 23. To calculate the flow number of each atomizer, the mass flow rate was measured using a "catch and weigh" method at various pressures throughout the range of testing. A series of five consecutive measurements were made at each pressure and averaged to determine the atomizer flow number at each point. To determine spray angle, each image in an image set was analyzed. The mean spray edge location at axial position y_1 and y_2 was used to calculate the spray cone half angle for each side of the spray. Spray angle from the left and right edge were then combined to determine the full spray cone angle. Key atomizer characteristics including the measured exit orifice diameter, atomizer flow number, and spray cone angle are shown in Table 1. Atomizer flow number and spray cone angle are plotted over the pressure ranges tested in Figure 24.

Table 1: Key Atomizer Characteristics

	Atomizer A	Atomizer B
Exit Orifice Diameter (d_o)	.0161"	.0164"
Pre-Filmer Surface Angle	N/A	58.8°
Flow Number @ 70 psi (FN_{US})	1.67	1.76
Spray Angle @ 70 psi (2θ)	59.8°	53.5°

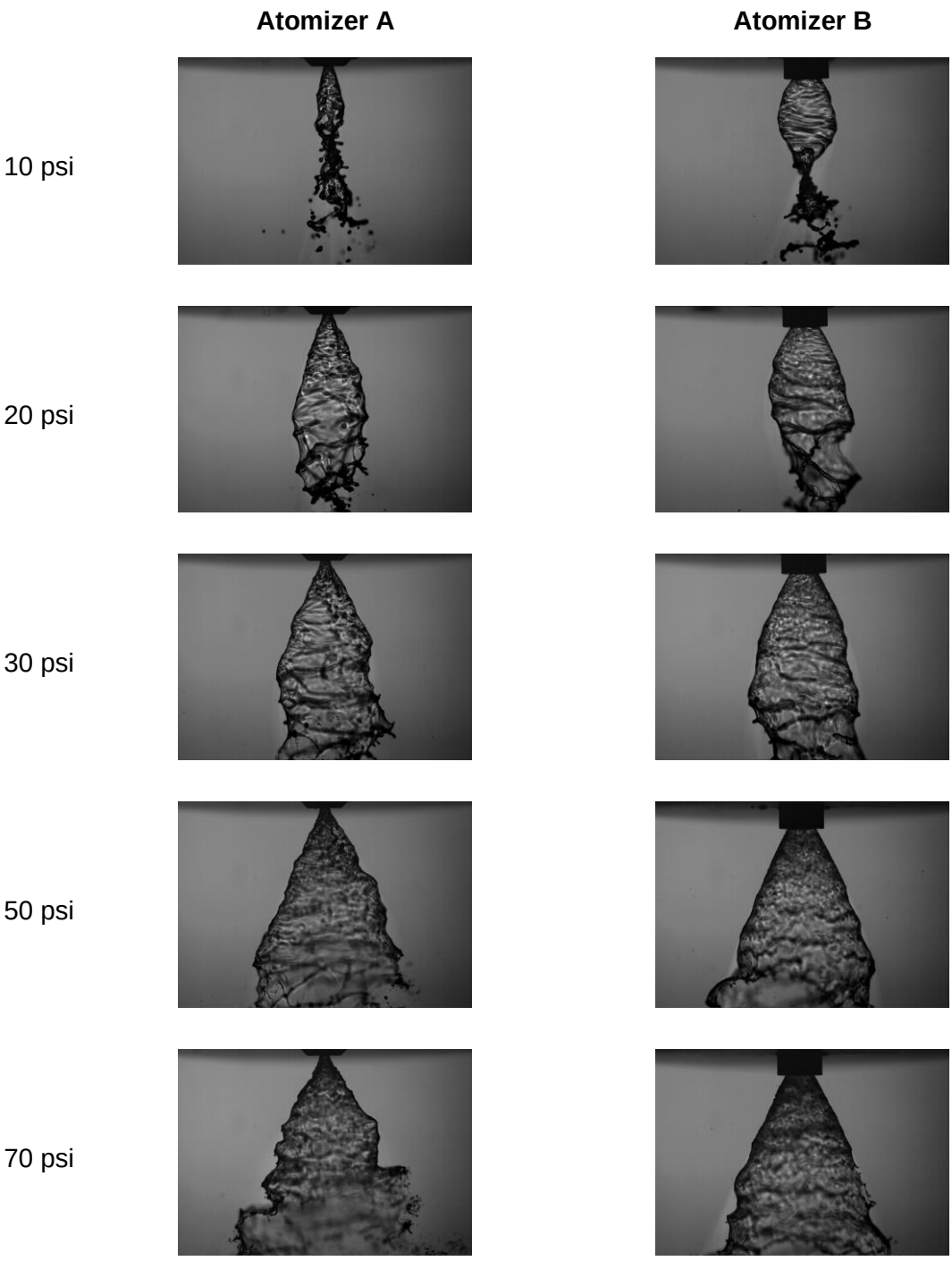

Figure 23: Atomizer A & B Side by Side Raw Spray Image Comparison

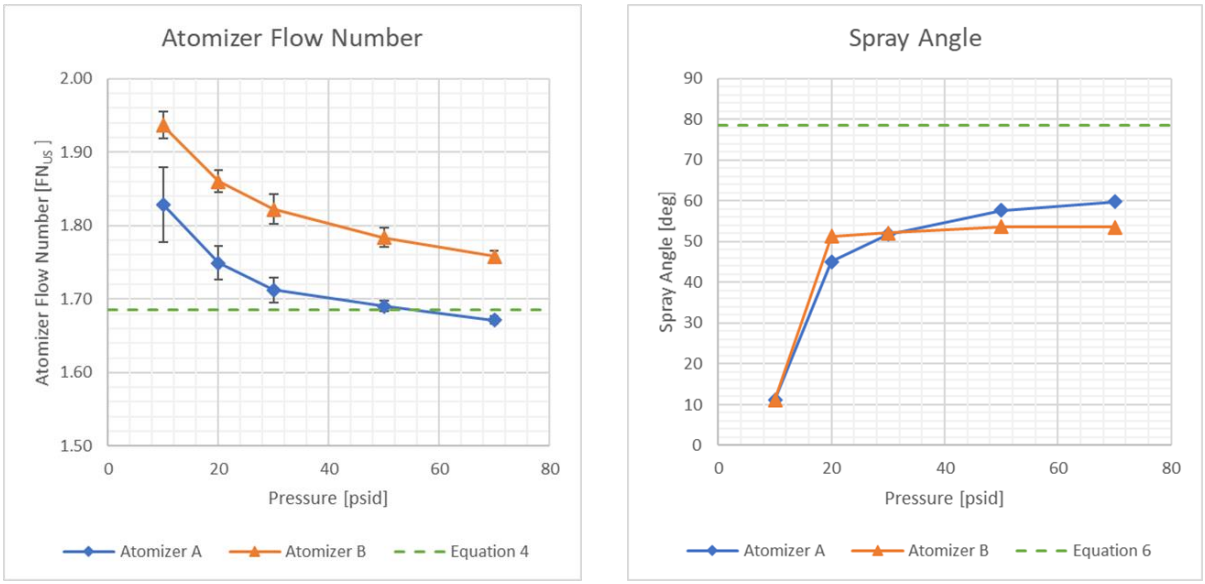

(a) (b)

Figure 24: Atomizer Flow Number (a) and Spray Angle (b) Over Pressure Range

It was found that the atomizer flow number for Atomizer B was consistently higher than Atomizer A. Based on Equation 4, due to inlet port area and swirl chamber diameter being identical (same swirl plug used in both atomizers), any changes to the flow number would be dependent on changes to the orifice diameter. Analytically, the flow number sensitivity due to the measured orifice sizes would predict a change in flow number increase of approximately 2.4%. Experimentally, the increase in flow number from Atomizer A to Atomizer B was observed to be 5.4% at 70 psid. It can be inferred that the additional increase in flow number is due to the addition of the pre-filming surface contributing to additional frictional losses and can be confirmed by the calculation of the atomizer discharge coefficient. The loss of energy as the fluid exits the orifice results in a larger film thickness size, thereby increasing the effective flow area of the atomizer and resulting in an increased atomizer flow number. This can also be substantiated by comparing the measured discharge coefficient and film thickness to the predicted values which represent an ideal atomizer with no frictional losses.

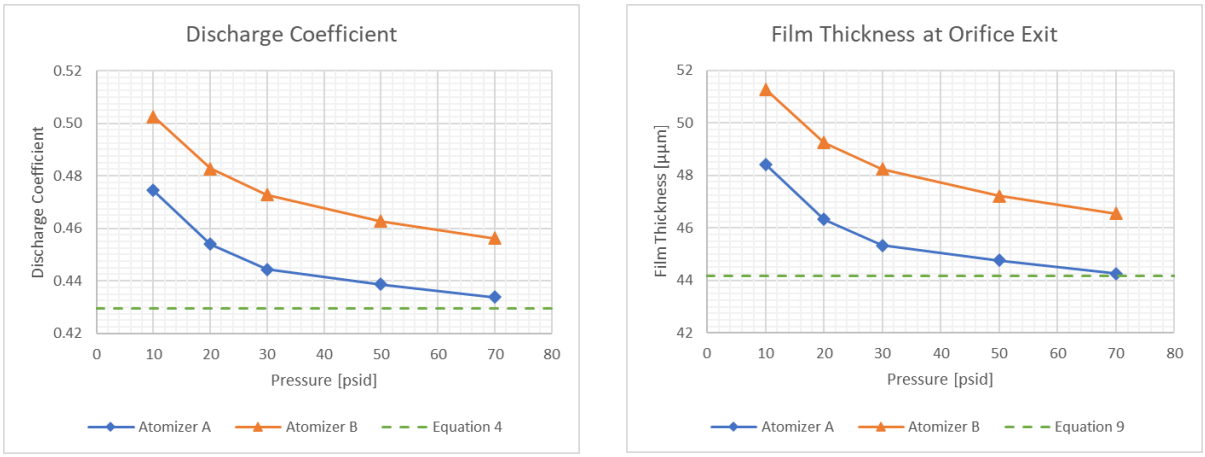

(a) (b)

Figure 25: Atomizer Discharge Coefficient (a) and Film Thickness (b) Over Pressure Range

For each atomizer, a series of 5 image sets were taken under steady operating conditions. Each image set was analyzed individually before being averaged together to determine the nominal spray edge position. For Atomizer A, 10 psid condition, 4 out of 5 images sets could not be analyzed due to poor spray quality. For Atomizer B, 20 psid condition, 1 image set demonstrated significant differences from the remaining 4. This was likely due to a setup error and so the image set was removed leaving 4 image sets to be used. The midpoint of the left and right edge nominal positions at 70 psid was selected as the centerline of the spray.

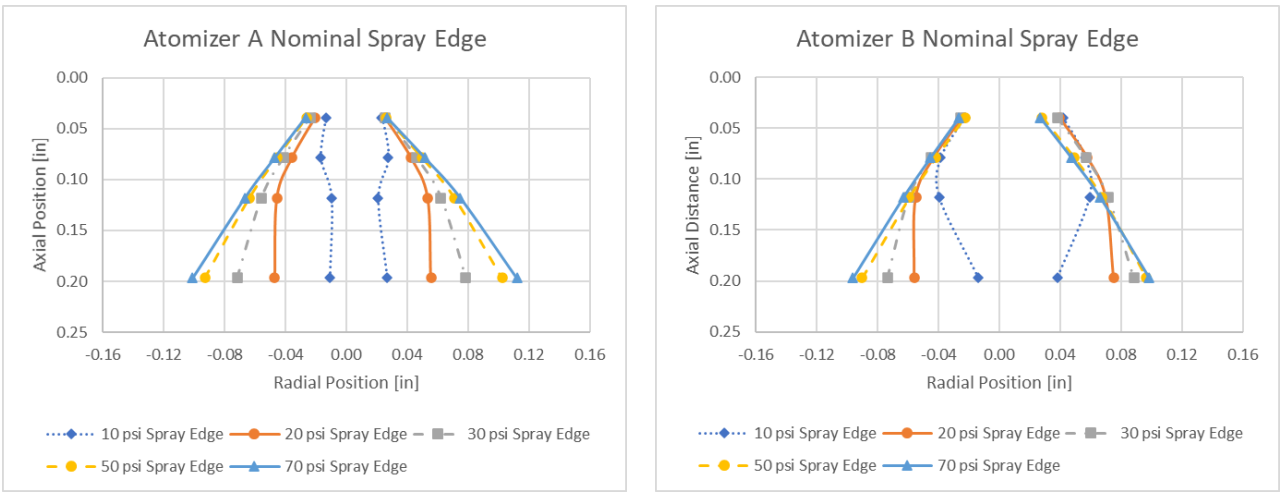

(a) *(b)*

Figure 26: Atomizer A (a) and Atomizer B (b) Nominal Spray Edge Position at Steady State Operating Conditions

All spray conditions for Atomizer A were completed in series without the atomizer being removed from the test setup. During the collection of image sets for Atomizer B, a fixture leak was identified before completion of the 50 psid and 70 psid image sets. The cause of the leak was determined to be an o-ring. The o-ring was replaced to resolve the issue, however this resulted in the atomizer being removed from the test setup. Since the test setup does not include a clocking feature to prevent rotation of the atomizer, the orientation of the atomizer may have changed between the 10/20/30 psid image sets and the 50/70 psid image sets. This can be seen in the right edge of the Atomizer B spray where the y_1 & y_2 edge locations are shifted in the positive x-direction for the lower pressure spray image sets. Due to the objectives of this research being focused on the variation in the spray edge and not dependent on the nominal position, it was determined that this would not have a major impact on the results of this study.

The variation of the spray edge at steady state operating conditions is shown in Figure 27. Apart from the 10 psid operating condition, opposite trends can be observed in each atomizer. For Atomizer A, the standard deviation of the spray edge can be seen increasing with increasing fluid pressure. The opposite trend of decreasing standard deviation with an increasing fluid pressure is observed in Atomizer B. In the case of Atomizer A, the increasing spray edge variation with increasing fluid pressure matches expectations as an increased relative velocity to the surrounding air would drive an increase in the wave growth of the spray edge. The opposite being true for Atomizer B indicates that the spray edge variation was not driven by the relative velocity, but likely a result of the ability for the liquid sheet to separate from the trailing edge of the pre-filming surface. At lower fluid velocities, there would be an increased chance of fluid buildup at the trailing edge similar to what was demonstrated by Holz et al. [14] leading to a greater spread of the velocity direction of the fluid. In the case of higher fluid velocity conditions, there would be a cleaner separation from the pre-filming surface trailing edge resulting in a more consistent fluid velocity direction.

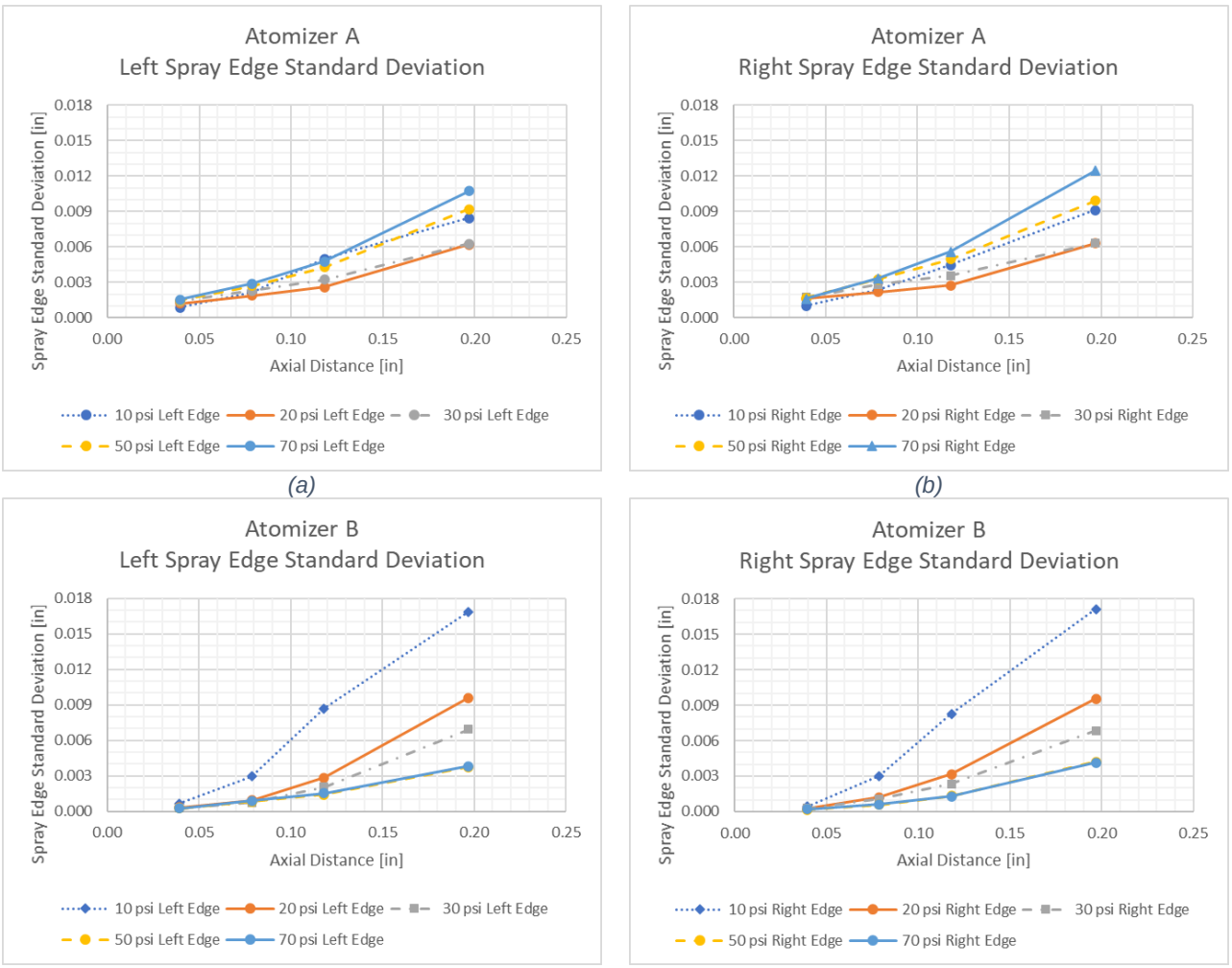

Figure 27: Atomizer A (a) and Atomizer B (b) Nominal Spray Edge Variation at Steady State Operating Conditions

The fluid velocity and Reynolds number calculated using Equation 13 and Equation 14 based on the measured parameters for each atomizer is shown in Figure 28.

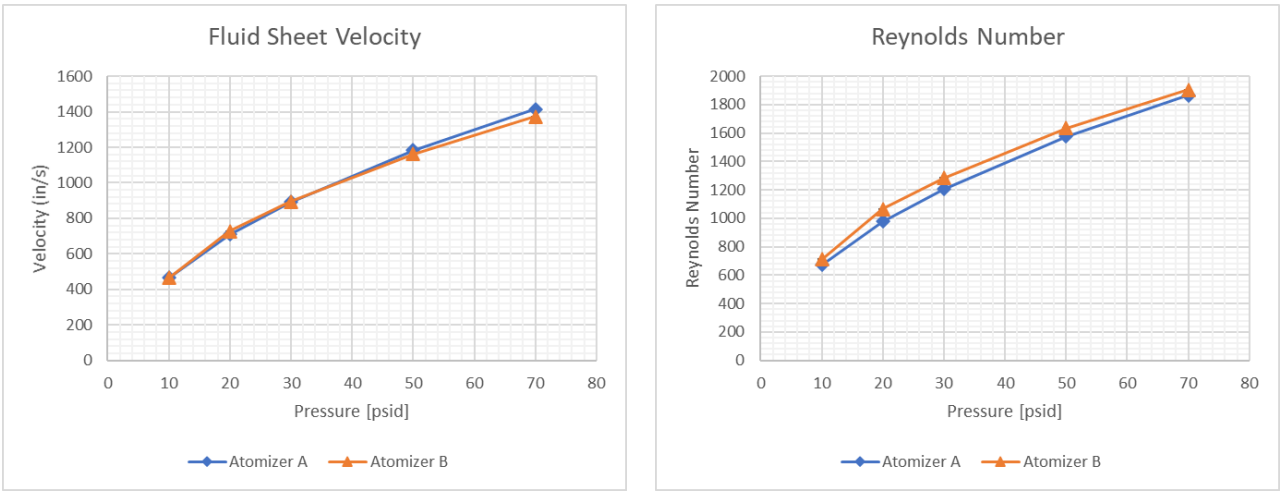

(a) *(b)*

Figure 28: Atomizer Fluid Sheet Velocity (a) and Reynolds Number (b) at Atomizer Exit

6.2 Atomizer Characterization Under Pressure Oscillations

During testing requiring pressure oscillation, the vibration apparatus was used to control frequency and amplitude of the pressure applied to the atomizer. Figure 29 demonstrates pressure measurement at various nominal pressures with 5, 10, and 15% peak to peak pressure variation. Pressure oscillation was applied at a frequency of 50 Hz. Due to limitations of the test setup, higher frequency levels were not achievable while generating a sufficient peak to peak pressure variation. It was observed that at low pressure and high peak to peak variation there was a saddle point in the descending pressure curve. This was likely the result of system dynamics of the fluid lines.

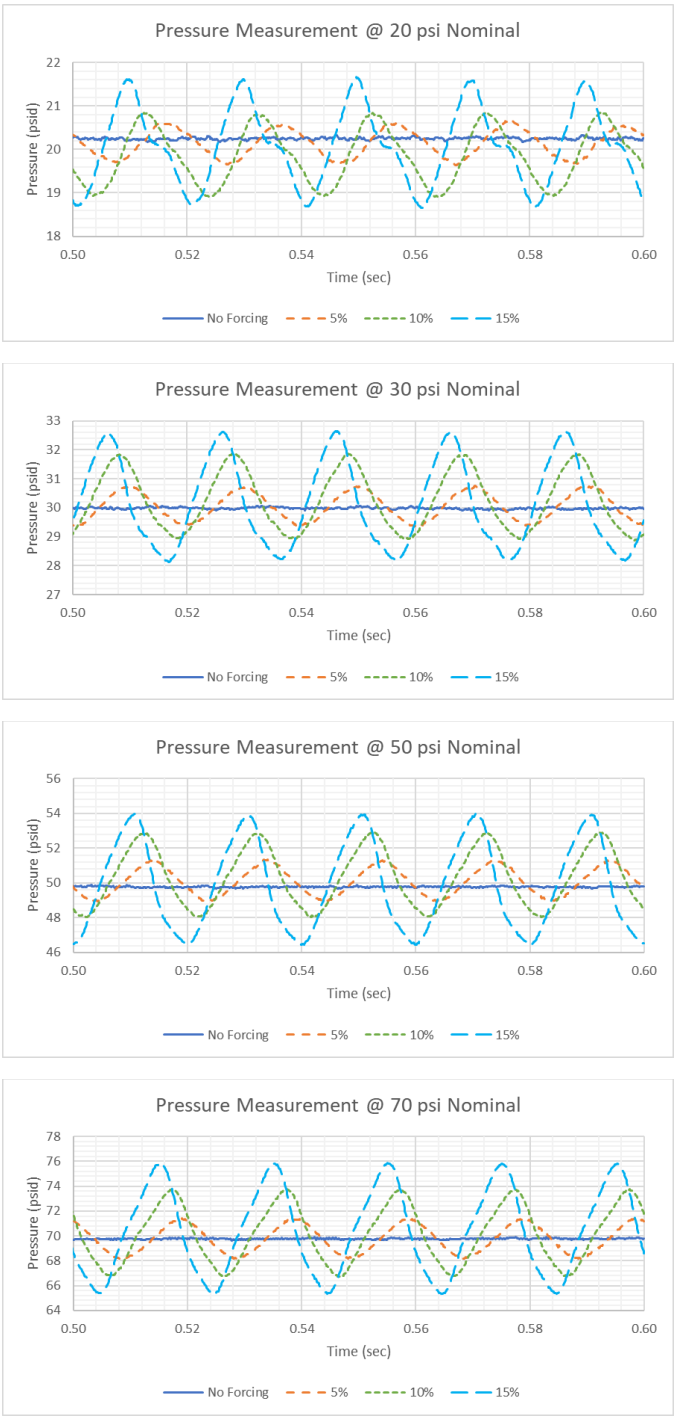

Figure 29: Pressure Measurement with Pressure Oscillation Applied at Various Nominal Pressures

The first objective during the pressure oscillation portion of testing was to compare the nominal position of the spray edge without pressure oscillation to the position under various levels of pressure oscillation. Figure 30 and Figure 31 show the nominal spray edge position for Atomizer A and B respectively. Error bars were plotted for the baseline spray condition (no pressure oscillation) and represent a 6-sigma confidence level based on the standard deviation of the sprays reported in the previous section. It can be observed that there is no appreciable change in the nominal position of the spray edge due to the application of pressure oscillation.

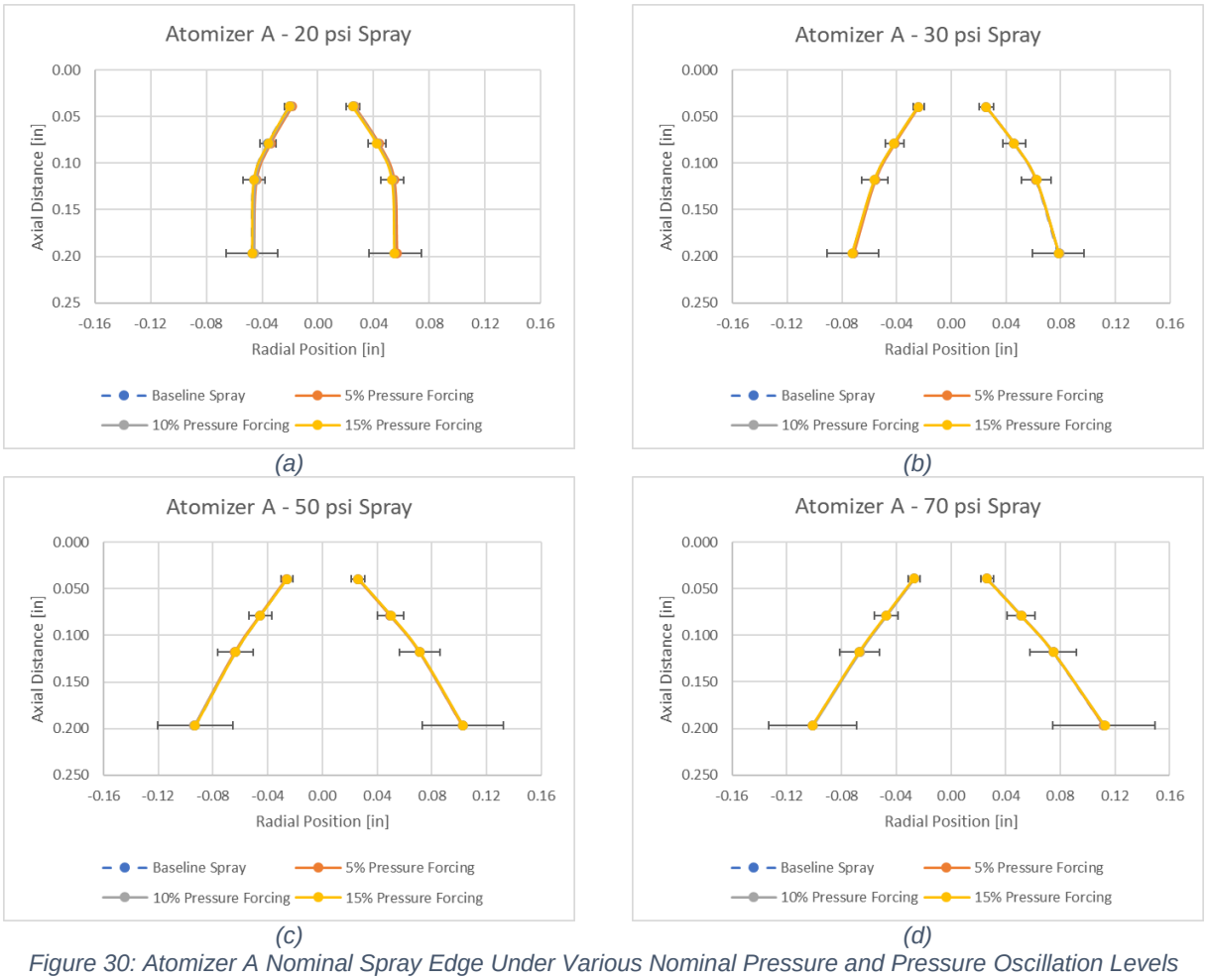

Figure 30: Atomizer A Nominal Spray Edge Under Various Nominal Pressure and Pressure Oscillation Levels

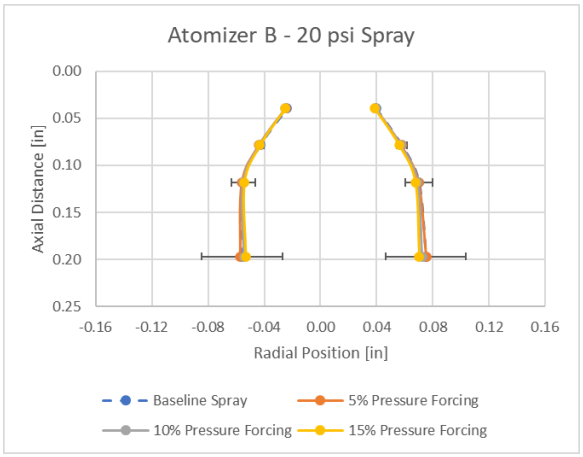

(a)

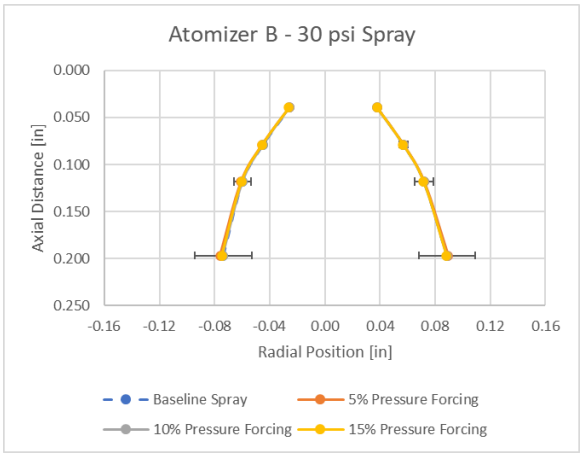

(b)

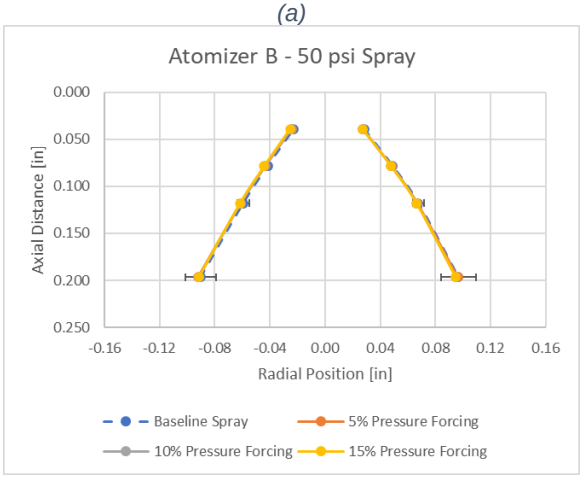

(c)

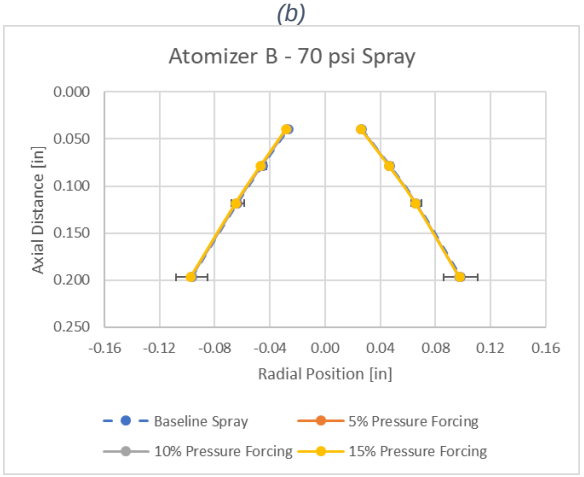

(d)

Figure 31: Atomizer B Nominal Spray Edge Under Various Nominal Pressure and Pressure Oscillation Levels

Next, the variation of each spray edge was examined against the various levels of pressure oscillation. To evaluate, pressure conditions without pressure oscillation were used to establish a baseline. At each pressure condition, a single data set was taken for each pressure oscillation level. A percent change was calculated using the baseline no pressure oscillation condition average. No significant trends were observed in Atomizer A (Figure 32) suggesting that the pressure oscillation had no impact on the edge of the spray. When examining the spray for Atomizer B (Figure 33), it was found that there was a significant increase in spray edge standard deviation at the axial position y = 0.039" (nearest to atomizer exit). This was most evident in the right edge of the spray. This trend was not observed in the left edge of the spray for the lower pressure (20 & 30 psi) condition however it was seen in the higher pressures. This could be a result of geometric factors that were rotated out of view when the atomizer was removed from the setup. Although this increase in spray edge variation was observed at the axial position nearest to the atomizer exit, it was not observed further downstream. It was hypothesized that the superposition of fluid imparted by the varying pressure was sizable enough to have an effect on the spray near field to the atomizer exit but dissipated in the liquid sheet prior to reaching the evaluation points further downstream. To test this hypothesis, Atomizer A was evaluated at an additional measurement point at y = 0.008" for the spray conditions of 50 and 70 psid. The additional measurement location is shown in Figure 34. The resulting spray variation demonstrated the same phenomenon observed in Atomizer B on both sides of the spray of Atomizer A confirming that the superposition of the fluid dissipates as the liquid sheet progressed further downstream. The spray variation of Atomizer A with the additional axial measurement location is shown in Figure 35.

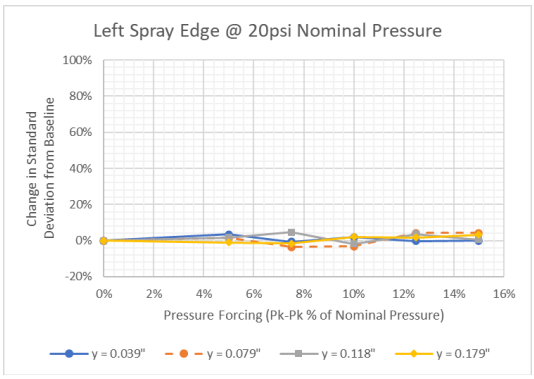

(a)

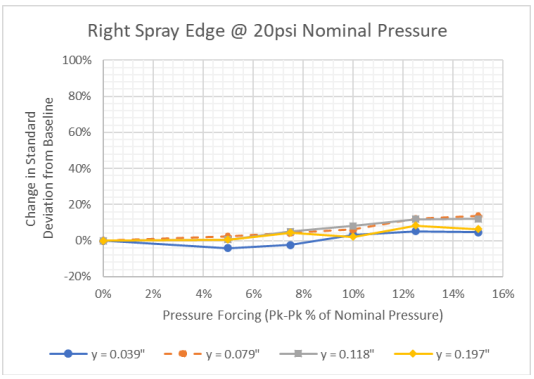

(b)

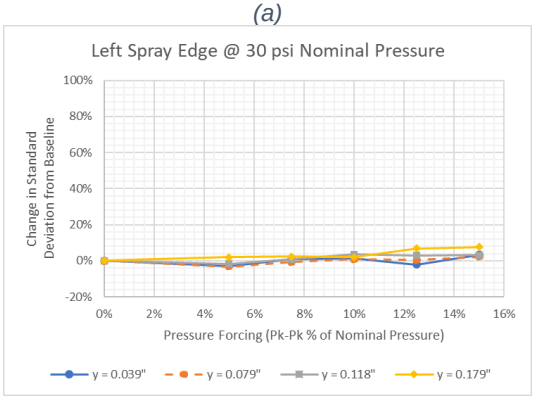

(c)

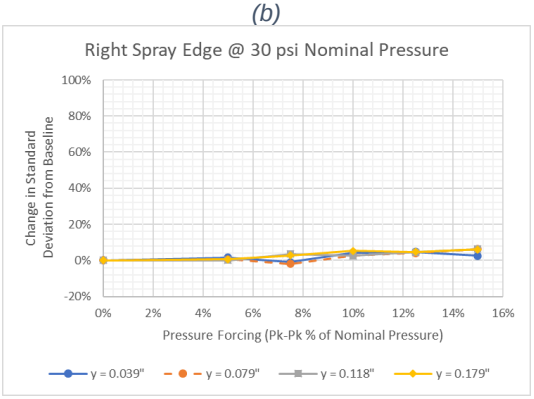

(d)

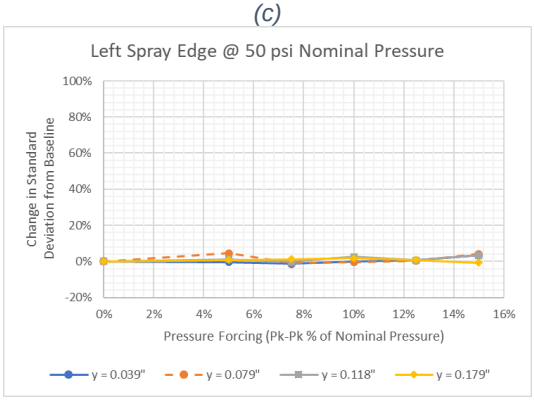

(e)

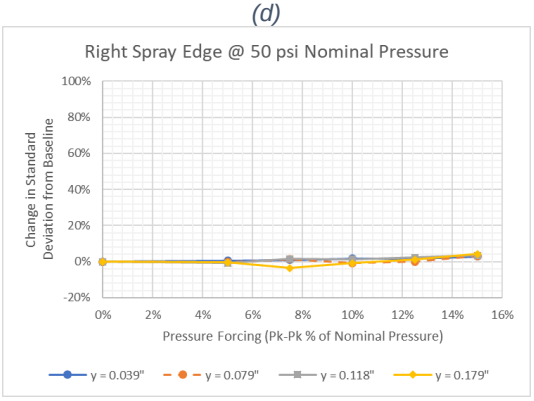

(f)

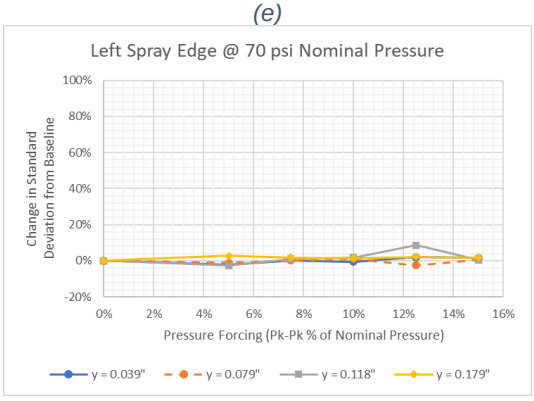

(g)

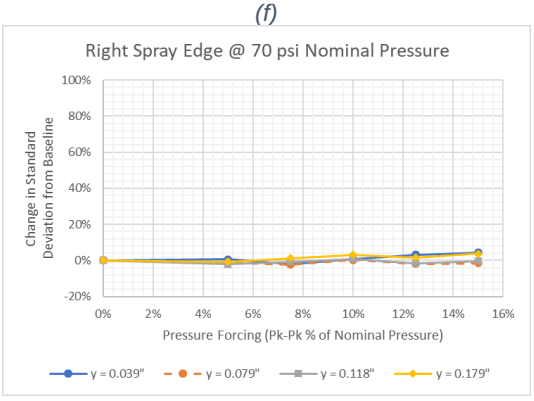

(h)

Figure 32: Atomizer A Spray Edge Variation Under Nominal Pressure and Various Pressure Oscillation Levels

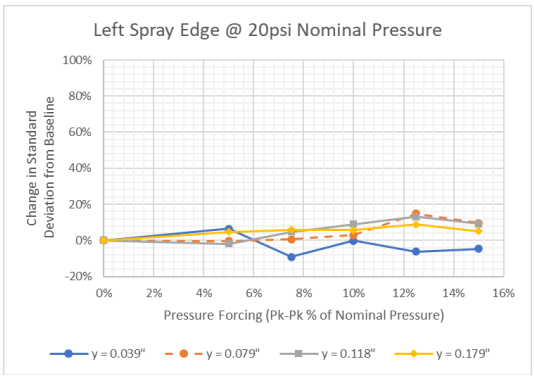

(a)

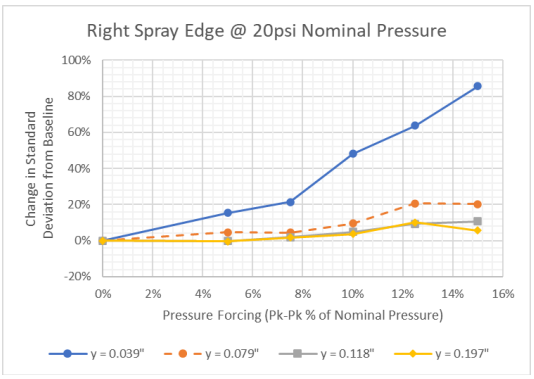

(b)

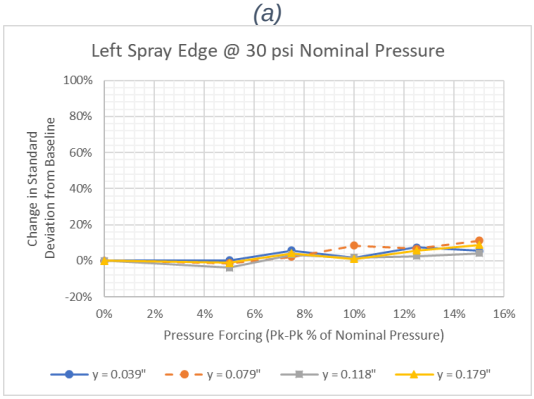

(c)

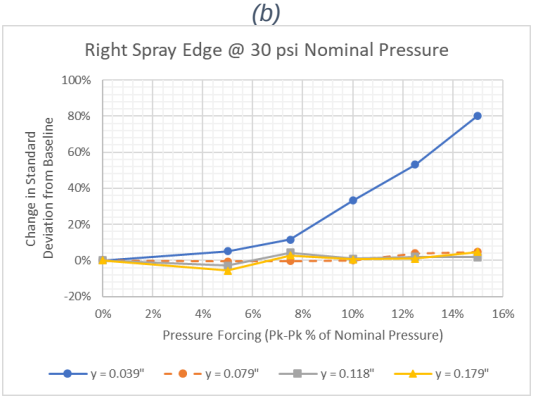

(d)

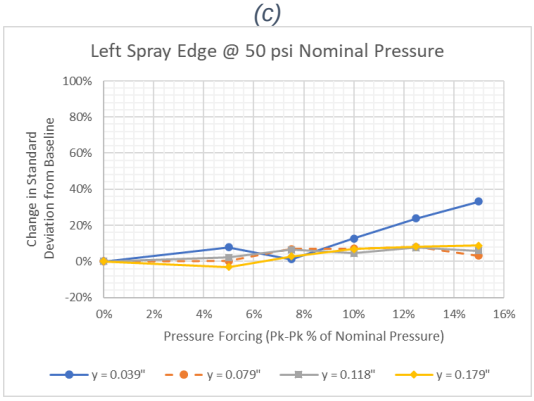

(e)

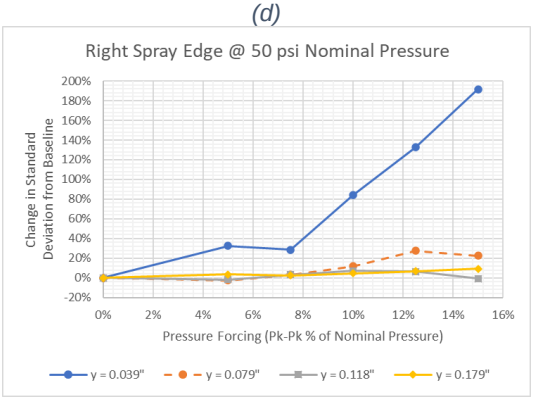

(f)

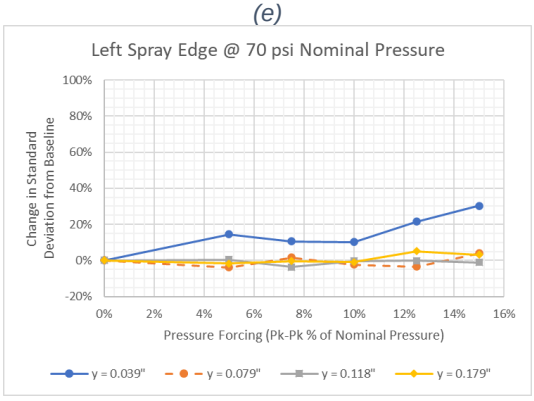

(g)

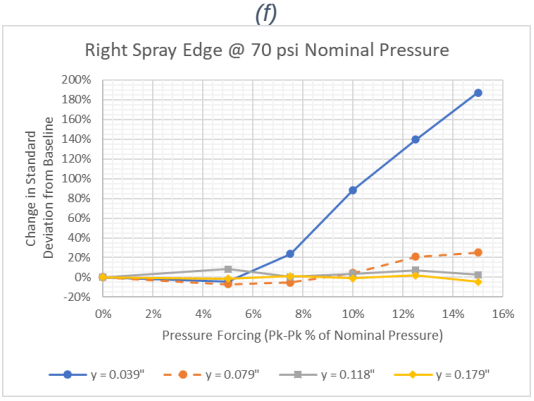

(h)

Figure 33: Atomizer B Spray Edge Variation Under Nominal Pressure and Various Pressure Oscillation Levels

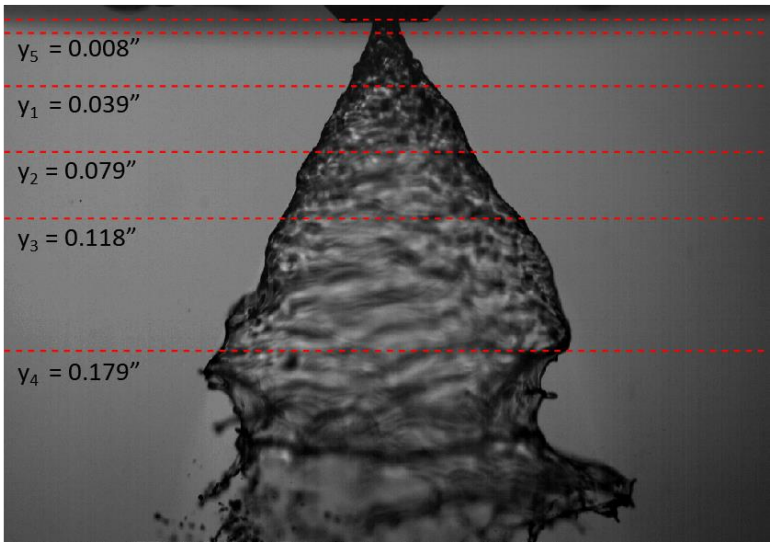

Figure 34: Atomizer A Spray Measurement Locations with Additional Position y5

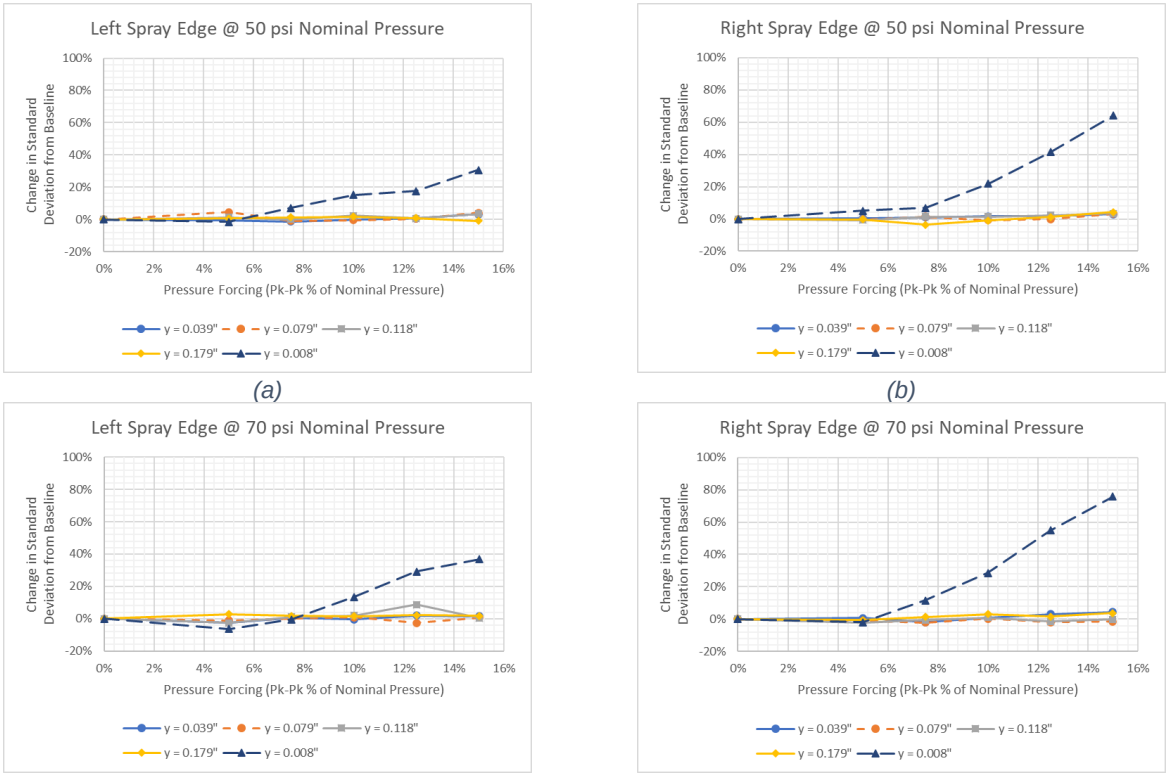

Figure 35: Atomizer A Nominal Spray Edge Under Various Nominal Pressure and Pressure Oscillation Levels with Additional Axial Distance Measurement Location

7.0 Conclusions

The intent of this work was to study a pressure-swirl atomizer under steady state operation and oscillating pressure differential conditions to simulate a dynamic system input to the atomizer. Atomizer spray with and without the addition of a pre-filming surface was evaluated to determine the influence that a pre-filming surface has on the dynamic response of the liquid sheet near the atomizer exit. High-speed video was utilized to capture the response of the liquid sheet and quantify the instability. It was found that under steady state operating conditions, the pre-filming surface increased the atomizer flow number and discharge coefficient. When comparing spray edge variation, the atomizer without a pre-filming surface demonstrated an increasing spray edge variation with increasing pressure while the opposite trend was observed in the atomizer with a pre-filming surface. Under conditions with an oscillating pressure differential, additional spray edge variation was observed near field to the atomizer exit but was nonexistent further downstream indicating that superposition of the fluid from pressure oscillation dissipated as it moved further from the atomizer exit and did not have an impact on wave growth in the liquid sheet.

For future studies with aerospace application, it would be beneficial to study the effect of oscillating pressure while using calibration fluid in place of water. Calibration fluid is typically used due to its similarities to the aviation fuel Jet-A. One notable difference between Jet-A and water is the surface tension, which for water is almost 3-times that of calibration fluid [9]. In the case of this study, the surface tension of water was likely a driving factor for the dissipation of the fluid particle superposition imparted by the pressure oscillation. In the case of calibration fluid, the pressure oscillation levels used in this study may be significant enough to induce sheet breakup closer to the nozzle exit.

Additionally, the use of a high-speed camera with sufficient FPS to capture the wave propagation as it moves downstream from the atomizer exit would provide valuable insight to the growth or decay of the waves in the liquid sheet. This research was limited to a spatial solution by the frame rate of the available camera. Previous studies have indicated that a frame rate in the magnitude of 10 kHz [2] would be required to deliver a temporal solution.

8.0 References

[1] A. H. Lefebvre and V. G. McDonell, *Atomization and Sprays*, Second Edi. Taylor and Francis Group, 2017.

[2] T. Marchione, C. Allouis, A. Amoresano, and F. Beretta, "Experimental Investigation of a Pressure Swirl Atomizer Spray," *J. Propuls. Power*, vol. 23, no. 5, pp. 1096–1101, 2007.

[3] K. U. Reddy and D. P. Mishra, "Studies on Spray Behavior of a Pressure Swirl Atomizer in Transition Regime," *J. Propuls. Power*, vol. 24, no. 1, pp. 74–80, 2008.

[4] H. Silva Couto, P. T. Lacava, D. Bastos-Netto, and A. P. Pimenta, "Experimental Evaluation of a Low Pressure-Swirl Atomizer Applied Engineering Design Procedure," *J. Propuls. Power*, vol. 25, no. 2, pp. 358–364, 2009.

[5] J. Xue, M. A. Jog, S. M. Jeng, E. Steinthorsson, and M. A. Benjamin, "Effect of Geometric Parameters on Simplex Atomizer Performance," *AIAA J.*, vol. 42, no. 12, pp. 2408–2415, 2008.

[6] B. Ahn, M. Ismailov, and S. Heister, "Experimental Study Swirl Injector Dynamic Response Using a Hydromechanical Pulsator," *J. Propuls. Power*, vol. 28, no. 3, pp. 585–595, 2012.

[7] H. Y. Kim, S. C. James, S. Y. Oh, S. S. Yoon, and E. J. Lee, "Measuring air core characteristics of a pressure-swirl atomizer via a transparent acrylic nozzle at various Reynolds numbers," *Exp. Therm. Fluid Sci.*, vol. 34, no. 8, pp. 1475–1483, 2010.

[8] Q. F. Fu, "Numerical simulation of the internal flow of swirl atomizer under ambient pressure," *Proc. Inst. Mech. Eng. Part C J. Mech. Eng. Sci.*, vol. 230, no. 15, pp. 2650–2659, 2016.

[9] H. C. Simmons and C. F. Harding, "Some Effects of Using Water as a Test Fluid in Fuel Nozzle Spray Analysis," *J. Eng. Power*, vol. 103, no. 1, p. 118, 2009.

[10] A. YANG, S. YANG, Y. XU, and L. LI, "Periodic atomization characteristics of simplex swirl injector induced by klystron effect," *Chinese J. Aeronaut.*, vol. 31, no. 5, pp. 1066–1074, 2018.

[11] N. Majumdar and M. S. Tirumkudulu, "Dynamics of Radially Expanding Liquid Sheets," *Phys. Rev. Lett.*, vol. 120, no. 16, p. 164501, 2018.

[12] V. Bazarov and V. Yang, "Liquid-Propellant Rocket Engine Injector Dynamics," *J. Propuls. Power*, vol. 14, no. 5, pp. 797–806, 1998.

[13] H. B. Squire, "Investigation of the instability of a moving liquid film," *Br. J. Appl. Phys.*, vol. 4, no. 6, pp. 167–169, 1953.

[14] S. Holz *et al.*, "New Insights in the Primary Breakup Process of Prefilming Airblast Atomizers by SPH Predictions Institut für Thermische Strömungsmaschinen (ITS), Karlsruher Institut für Technologie (KIT), Germany," pp. 1–8, 2018.

[15] J. D. Lee, A. Saha, S. Basu, and R. Kumar, "Effects of Injection Pressure on Spray Atomization Characteristics with Measurement Technique Cross-Validation University of Central Florida , Orlando , USA Indian Institute of Science , Bangalore , USA," *12th Trienn. Int. Conf. Liq. At. Spray Syst. 2-6 Sept.*, pp. 1–8, 2012.

[16] J. Santner and H. Stone, "Santner Waves.pdf." [Online]. Available: http://www.princeton.edu/~stonelab/Teaching/Santner Waves.

9.0 Appendix

Derivation of Flow Number as defined by Equation 5

Mass flow rate can be defined as follows

$$\dot{m} = V * A * \rho * C_d$$

Substituting the solution for mass flow rate into Equation 1 yields

$$FN_{US} = \frac{V * A * \rho * C_d}{\sqrt{\Delta \mathrm{P}}}$$

Velocity can be defined using Bernoulli's Equation with a constant potential

$$\frac{V_1^2}{2g} + \frac{P_1}{\gamma} = \frac{V_2^2}{2g} + \frac{P_2}{\gamma}$$

$$V_2 = \sqrt{\frac{\Delta P * 2g}{\gamma} + V_1} \qquad \text{Where } V_1 = 0$$

Substituting velocity into the flow number equation yields

$$FN_{US} = \frac{\sqrt{\frac{\Delta P * 2g}{\gamma}} * A * \rho * C_d}{\sqrt{\Delta P}}$$

After including units and conversion terms, the flow number equation can be rewritten as follows

$$FN_{US} = 2406.51 * \mathrm{A} * C_d * \sqrt{\rho}$$

For convenience, the equation is rewritten to use specific gravity instead of fluid density

$$FN_{US} = 19000 * A_o * C_d * \sqrt{s}$$

Where:

V	Fluid Velocity [ft/sec]
P	Fluid Pressure [psi]
γ	Specific Weight [lbf/ft^3]
g	Standard Acceleration of Gravity [ft/sec^2]
ρ	Fluid Density [lbm/ft^3]
A	Geometric Area of Flow Area [in^2]
FN_{US}	Flow number [$(lbm/hr)/\sqrt{psi}$]
C_d	Coefficient of Discharge [$dimensionless$]
s	Specific Gravity [$dimensionless$]